Water Resources Research

RESEARCH ARTICLE
10.1029/2019WR025743

Special Section:
Coastal hydrology and oceanography

The Propagation of Fluvial Flood Waves Through a Backwater-Estuarine Environment

S. L. Dykstra[1,2] and B. Dzwonkowski[1,2]

[1]Department of Marine Sciences, Dauphin Island Sea Lab, University of South Alabama, Dauphin Island, AL, USA, [2]Dauphin Island Sea Lab, Dauphin Island, AL, USA

Key Points:
- Observations demonstrate river (fluvial) flood waves can fully transit a coastal system through the fluvial-marine transition to the sea
- Analysis of the momentum balance in the backwater region of the system identified dynamical transitions associated with system morphology
- Flooding caused large discharge events to slow and attenuate, significantly impacting estuarine water level, velocity, and flushing

Supporting Information:
- Supporting Information S1
- Table S1

Correspondence to:
S. L. Dykstra,
sdykstra@disl.org

Citation:
Dykstra, S. L., & Dzwonkowski, B. (2020). The propagation of fluvial flood waves through a backwater-estuarine environment. *Water Resources Research*, *56*, e2019WR025743. https://doi.org/10.1029/2019WR025743

Received 17 JUN 2019
Accepted 23 DEC 2019
Accepted article online 26 DEC 2019

Abstract Coastal cities and ports are located along estuaries and deltas where flooding from rivers can be as devastating as storm surges. Precise river discharge measurements are taken far inland of marine influences and backwater environments, creating large timing and magnitude uncertainties downstream at the coast. Long-term discharge, water level, velocity, and salinity measurements in coastal Alabama were used to observe the timing and magnitude of discharge events flowing 238 km from rivers to the Gulf of Mexico as river flood (fluvial) waves. Waves were described and simplified using a momentum balance, phasing techniques, and wave theory from inland rivers. Results showed the coastal backwater environment transitioned to a drawdown (i.e., plunging water profile) at bankfull discharge and suggested the drawdown location and intensity was strongly influenced by the frictional transition of the delta from tupelo-cypress forest to oligohaline marsh. The horizontal (velocity) and vertical (water level) components of fluvial waves were observed propagating through this dynamic deltaic-estuarine environment transitioning from in phase diffusive waves to out of phase dynamic waves. The wave celerity increased with surface water slope and decreased with cross-sectional area. Instead of larger events propagating faster, the geometry (i.e., levees and floodplains) and flooding significantly delayed and attenuated the magnitude of discharge reaching the gulf. This flooding downstream of discharge measurements modulated the estuarine water level, velocity, and flushing of salt. The use of fluvial wave theory will increase the precision of coastal flooding predictions for stakeholders and research now, as well as under future sea level rise.

Plain Language Summary Most coastal cities and ports are located along rivers near the sea and are increasingly vulnerable to flooding from both sources due to intense development and sea level rise. River discharge is measured far inland where deltas, estuaries, and marine forces do not interfere, but these same influences make it difficult to observe when and how much flooding occurs near the coast. Usually in rivers, large flooding events move from upstream to downstream faster than small events. A study was conducted to track flooding events through a coastal environment using long-term observations in Alabama. In contrast to flooding behavior in rivers, the results showed small flooding events moved downstream faster than large events. This occurred because large events caused water to flow out of the river channel, spilling over the forested floodplains where it traveled more slowly. This flooding of the delta also decreased the impact of large events and demonstrates large river discharge events can be tracked in coastal areas. These findings indicate stakeholders can decrease the intensity of coastal flooding and provide more time to prepare by allowing inland regions of rivers to flood and/or by managing vegetation type, both of which reduce the downstream height of water.

1. Introduction

Compound flooding events from storm surge and river discharge are intensifying in coastal communities from sea level rise. Even small floods (i.e., nuisance flooding) put stress on infrastructure, cause socioeconomic damage, and threaten water security (Ghanbari et al., 2019; Moftakhari et al., 2018). Today, 40% of the world's population lives near the coast (<100 km) with the highest concentrations near low-lying rivers that also contain most of the world's ports (e.g., Shanghai, Dhaka, and New York; United Nations, 2017). River discharge (herein discharge) is reliably measured inland of tides, estuaries, and deltas where long backwater regions O (Order of magnitude 10–1,000 km) can significantly impact flow while altering the downstream dynamics of estuarine and coastal systems. Accurate measurements of discharge (i.e., timing and magnitude) accounting for this fluvial-marine transition are needed for coastal communities.

Coastal flooding is commonly observed with long marine waves propagating inland from tides or setup from wind (e.g., storm surge) first raising the water level in the sea before raising inland waters. These waves have a vertical component modifying the water level and a horizontal component changing velocity. The amplitude and celerity of long waves are modulated by friction and local geometry (e.g., cross-sectional area). This can also force the horizontal and vertical wave components to propagate out of phase (Hoitink & Jay, 2016). Another type of long wave has recently been identified in the coastal environment from hydroelectric power peaking on the Columbia River, but this wave moves seaward in the opposite direction of marine waves. The unnatural disturbance is described as a "pseudo-tide" due to a similar amplitude and frequency as the diurnal tide (Jay et al., 2016). Rivers also have long waves that propagate seaward but, from natural precipitation events, first raising the water levels upstream before causing a delayed rise downstream. These river flood waves, or fluvial waves, have not been clearly reported in the coastal environment even though flooding discharge events have been observed in estuaries raising water levels and increasing the seaward velocity of water (Hoitink & Jay, 2016).

The propagation of a fluvial wave is strongly influenced by local geometry. As rivers approach the coast, the bed and surface water slope diverge forming a M1 profile (M: mild bed, 1:diverging; Chow, 1959) described as a backwater environment where depth increases and water slows. This initially increases sediment deposition before decreasing and fining seaward. The typical bed profile slopes upward near the coast and has been observed in tidal and nontidal systems (e.g., Laurentian Great Lakes, Lane, 1957; Mississippi River, Nittrouer et al., 2012; Kapuas River, Kästner et al., 2017). Nittrouer et al. (2012) state backwater environments can be found in all coastal lowland river systems, but Gugliotta and Saito (2019) question the application of backwater theory in tidal environments because their results suggest the typical profile is formed at least in part by tides and did not require a drawdown.

A drawdown forms if the surface and bed slopes converge (M2, 2:converging), causing the water level profile to steepen and water to accelerate in the downstream direction. This occurs at coastlines during high discharge due to lower friction fixing the water level near 0 m (Lane, 1957) scouring the bed and transporting sediments seaward of the river mouth (Chow, 1959). The M1-M2 transition is caused by nonuniform flow (i.e., change in discharge) and is the foundational process controlling fluvial-deltaic stratigraphy (Ganti et al. 2016a). While field observations of the transition are limited, Lamb et al.'s (2012) model of the Mississippi River channel suggests the transition occurs at bankfull discharge but was not able to demonstrate this without overbank conditions. These dynamics and geometry may significantly impact how fluvial waves propagate.

Backwater environments strongly influence the geometry of the entire fluvial-marine transition. The size of a backwater is approximated with the backwater length ($L_b = h^* {S_b}^{-1}$; h, and S_b are height and bed slope), extending from the lowest point on the bed profile (usually inland of the river mouth) to the location where the bed slope intersects sea level. Along L_b, inland meandering rivers decrease in lateral migration forming thicker deposits and large levees (Fernandes et al., 2016). The levees can be scoured during overbank flow and form small crevasses, gaps that allow the water to exchange with the floodplain during lower discharge conditions. Complete destruction of the levee allows the river to avulse or change directions (Chatanantavet et al., 2012). L_b directly relates to the drawdown length ($L_d = 0.5L_b$; Lamb et al., 2012) and scaling of an entire delta. Ganti et al., (2016a) show with lab experiments how the morphology of a prograding delta scales with L_b for peak erosion, deposition, and avulsion ($x \approx 0.25L_b$, $x \approx 0.35L_b$, and $x \approx 0.45L_b$, respectively, where x is the distance inland). The delta apex (i.e., opening of the delta plain) on the other hand is fixed by antecedent geology and can also influence how a delta scales with L_b (Hartley et al., 2016).

Backwater conditions enable the marine environment to penetrate far inland with tides and salt, creating ecological zonation with frictional feedbacks. Most tidal river freshwater wetlands are deciduous forests, while saltwater wetlands are predominantly grasses in temperate climates or mangroves in tropical climates (Ensign et al., 2014; Gugliotta et al., 2017). Grasses have flexible structure that bend under the pressure of flowing water and become easily submerged while trees are rigid and are rarely submerged. These differences are observed in the friction acting on flow as it reaches riparian zones and moves through floodplains (Hamill, 1983; Yang et al., 2007). Friction from vegetation can also attenuate and slow fluvial waves but has less influence as friction increases (Anderson et al., 2006). Studies of the M1-M2 transition

have not considered the impact of vegetation (e.g., Chatanantavet et al., 2012; Gantiet al., 2016a; Lamb et al., 2012) even though it represents an important frictional component that could form an M2 profile.

The magnitude and timing of discharge is commonly estimated with rudimentary methods and poor assumptions even though it is critical to the understanding of estuarine and shelf circulation, biogeochemical cycles, and ecology (Dzwonkowski et al., 2018; Hopkinson & Vallino, 1995). Traditionally, the magnitudes from discharge measurements taken far inland are applied near the coast without adjustments (e.g., Nittrouer et al., 2012) or use a multiplier based on the change in watershed size (e.g., Gisen & Savenije, 2015). The timing of discharge is often assumed to be the same as at the inland measurement or is lagged with a constant time delay (e.g., Dzwonkowski et al., 2015). However, most estuarine studies do not mention if or how they account for these adjustments. New approaches to estimate coastal discharge calibrate a rating curve with water level and velocity measurements (e.g., Hoitink et al., 2009; Kästner et al., 2018; Ruhl & Simpson, 2005) or use the damping effects of discharge on tides (e.g., Matte et al., 2018; Moftakhari et al., 2013). The former is limited to fluvial dominant regions and in channel flow, usually lacking calibration for high discharge events. The latter lacks temporal precision O (week) and is best used to reconstruct gappy upstream discharge records (Hoitink & Jay, 2016; Moftakhari et al., 2016). By contrast, inland of marine influences, when nearby measurements are lacking, hydrologists take a dramatically different approach by estimating flow with routing methods that apply fluvial wave theory (e.g., Lighthill & Whitham, 1955; Cunge, 1969). The study of fluvial waves has stopped inland of marine influences, leaving a critical gap in our understanding of both fluvial and estuarine processes.

This study fills an important knowledge gap by observing the propagation of fluvial waves through the fluvial-marine transition using both water level and velocity measurements. Since fluvial-marine transitions are strongly influenced by backwater dynamics, a focus is placed on (1) identifying the hydrodynamic conditions and observing backwater-drawdown (M1-M2) transitions. Then, we (2) show the propagation of fluvial waves in the coastal environment, identifying changes in momentum, wave celerity and wave magnitude. Finally, we (3) examine broader insights by describing coastal discharge with a fluvial wave and discuss the application in other systems. We begin by describing fluvial wave theory.

2. Fluvial Wave Theory

The impact of a local environment on the movement of water and long wave motion (e.g., celerity and amplitude) can be identified using a momentum balance. The momentum of both fluvial and marine long waves is captured using the same one-dimensional Saint-Venant equations (i.e., shallow water equations; Dronkers, 1964). The equations are solved with mass conservation for the local subtidal momentum balance (similar to Losada et al., 2017):

$$\underbrace{\overline{gW\frac{|u|u}{C^2}}}_{\text{T1}}+\underbrace{\overline{gA\frac{\partial h}{\partial x}}}_{\text{T2}}-\underbrace{\overline{\left(2u\frac{\partial A}{\partial t}+u^2\frac{\partial A}{\partial x}\right)}}_{\text{T3}}+\underbrace{\overline{\frac{\partial Au}{\partial t}}}_{\text{T4}}+\underbrace{\overline{gA\frac{h\partial\rho}{\rho\partial x}}}_{\text{T5.}}=0 \tag{1}$$

Here g is gravity, W is width, u is velocity, C is the Chezy coefficient ($C = {h_0}^{1/6}/n$, n is the Manning number), A is cross-sectional area, h is height, x is longitudinal distance, t is time, ρ is density, and the bar indicates tidal averaging. The terms from left to right are friction (T1), pressure gradient (T2), acceleration (T3), storage (T4), and density gradient (T5), respectively. Storage and density gradient are often negligible and omitted to simplify the momentum balance.

The primary terms capturing long wave momentum are friction, pressure gradient, and acceleration. Wave momentum forms a wave type spectrum helpful for simplifying terms when the wave number is normalized by the water surface or bed slope (k^*):

$$k^* = \frac{2\pi}{\lambda}\frac{h}{S_0} \tag{2}$$

where λ is wavelength and S_0 is surface or bed slope. Wave types from small to large k^* values include diffusive waves with a friction-pressure gradient balance, dynamic waves with a friction-pressure gradient-acceleration balance, and gravity waves with a pressure gradient-acceleration balance. At the end of the

spectrum attenuation is low, but in the middle of the dynamic wave band attenuation peaks and celerity quickly changes with larger k* waves being an order of magnitude faster than smaller k^* waves (Ponce & Simons, 1977). Differentiating momentum is helpful because simpler diffusive waves have a celerity solution ($c = Ku$, where K is a constant derived as 3/2) that scales only with u, while dynamic waves propagate and attenuate faster making them more difficult to observe and describe (Ponce et al., 1978). Fluvial waves are diffusive, with a small k^*, and become dynamic as the bed slope decreases, a process that increases the acceleration relative to the other terms (Ponce, 1989).

Since the normalizing term for k^* is the calculation for L_b (i.e. h/S_0), k^* can be approximated in a backwater environment by rewriting equation (2):

$$k^* \approx \frac{L_b}{\lambda} \tag{3}$$

Thus, L_b and λ can be used to estimate wave type and the distribution of wave momentum. When λ is much longer than L_b ($\lambda >> L_b$) the wave is diffusive and the backwater effects are negligible. If $\lambda \approx L_b$, the wave may be dynamic and can be determined with analytical solutions using the Froude number at normal flow (i.e., $\mathrm{Fr} = u/\sqrt{gh}$ when the bed and water surface slope are the same). These solutions accounting for backwater effects are solved in Tsai (2005). Equation (3) is also a simple approximation for determining which solutions to use for celerity and attenuation (e.g., Ponce & Simons, 1977) but cannot capture the local effects like equation (1).

The primary local effects impacting diffusive wave momentum and propagation are geometry and friction. High friction, shallow slopes, and a large cross-sectional area attenuate and slow waves. These all cause a downstream peak discharge to be smaller and have a longer delay (Woltemade & Potter, 1994; Lininger & Latrubesse, 2016). Sometimes local effects interact. When a bed slope becomes shallow, friction can force the horizontal and vertical wave components out of phase. This alters a discharge-water level rating curve, the most common method used for calculating discharge, by creating hysteresis in the form of a loop with errors in discharge timing and magnitude (Dottori et al., 2009). Identifying changes in wave momentum and propagation from a local environment is critical for accurate discharge measurements.

3. Study Region: Coastal Alabama

Coastal Alabama provided a unique opportunity for this study with a high concentration of long-term data sets in a representative fluvial-marine transition (Figure 1 and Table S1 in the supporting information). In the Continental United States, the short Alabama coast has the fourth largest freshwater discharge, one of the largest deltas, and the tenth busiest port (American Association of Port Authorities, 2015; Smith et al., 2013). The Tombigbee and Alabama Rivers (watershed area: 51,921 and 58,896 km^2, respectively) deliver most of the water entering the delta and bay. The marine influence stops at the most seaward dams, 238 river kilometers (rkm) inland on both rivers, where tides can reach under low discharge and become amplified. At high discharge, river water flows over these dams like a weir. This distance is similar to other systems like the Columbia (234 rkm; Jay et al., 2016) and Hudson Rivers (240 rkm; Ralston & Geyer, 2017), but the rivers in this study form a delta.

The subaerial delta extends ~95 km from the Suwanee-Wiggins suture within a broad (10–20 km) pre-Holocene valley to the bayhead's current location, where it transgressed to 8,200 years before present (Figure 1; Greene et al., 2007; Rodriguez et al., 2008). The modern delta area is 1,370 km^2 when delineated at the 1-year recurrence interval of the water level or 2,010 km^2 using the alluvial Holocene deposits from Szabo et al. (1988). The Tombigbee and Alabama Rivers enter wide alluvial plains characteristic of an upper delta with a single channel at the suture (~190 rkm inland; Mancini et al., 1991). The plains and streams merge (122 rkm inland) forming a two-lobe upper delta plain and the Mobile River that flows into the lower delta. After 9.5 rkm, the largest bifurcation forms the Tensaw Distributary (east) with complex anastomosing channels and the Mobile Distributary (west) with two thirds of the water and one channel that continues downstream to the bayhead (~48 rkm inland). Well-developed natural levees line the channels, separating them from the subaerial plain, oxbow lakes, and network of flood basins (Robinson et al., 1956; Smith, 1988).

The lower delta is the most biodiverse location in temperate North America and has been designated as the Mobile-Tensaw River Bottomlands National Natural Landmark (Waselkov et al., 2016). Most of the delta is a

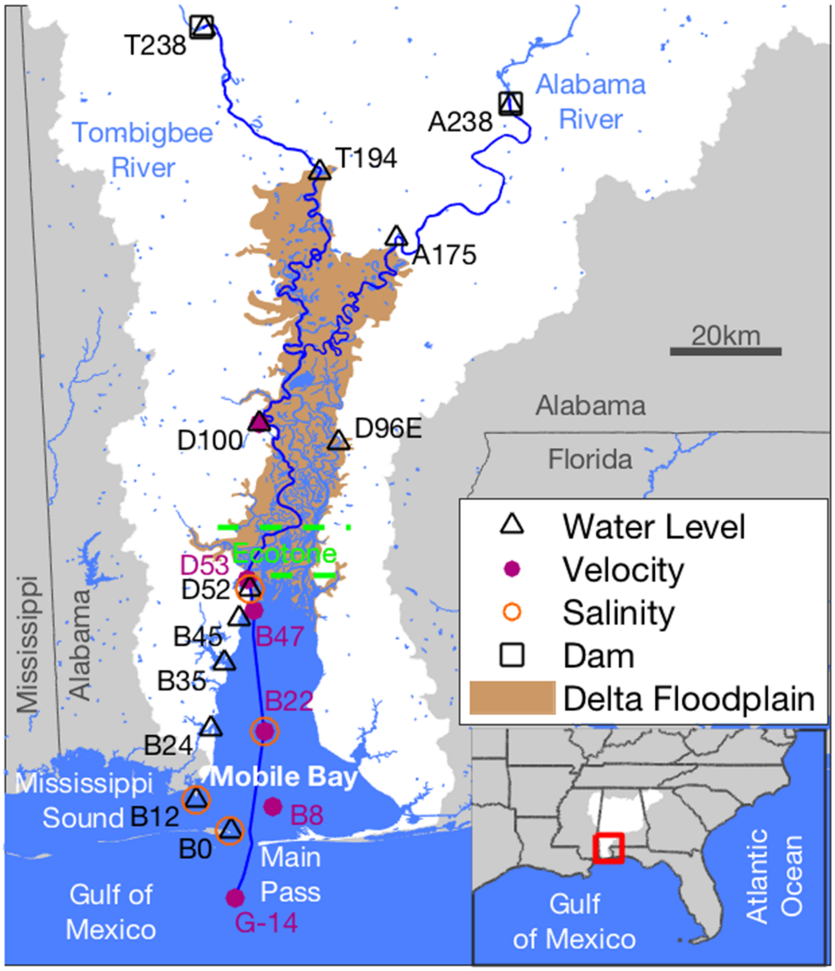

Figure 1. A map of the coastal region of Alabama with the location of the long-term stations used in this study. The Mobile Bay watershed is white and the longitudinal profile is shown with a dark blue line.

densely vegetated water tupelo-bald cypress (Nyssa aquatica and Taxodium distichum, respectively) tidal freshwater forest (PFO1F) that transitions to an oligohaline marsh (i.e., grasses; E2EM1P) 10- to 20-km north of the bayhead (Figure 1; Kidd et al., 2015; U. S. Fish and Wildlife Service, 2019). The lower delta is locally called the Mobile-Tensaw Delta after its distributaries. To include the upper delta and reflect common naming practices of deltas after the contributing streams (e.g., Ganges-Brahmaputra Delta and Mekong Delta), we refer to it as the Tombigbee-Alabama Delta (Tom-Al). The Tom-Al is similar in size and discharge to the Rhone (France), Krishna (India), and Copper (USA) deltas (Syvitski & Saito, 2007).

The delta flows into Mobile Bay, a bar-build drowned valley estuary typical of the Northern Gulf of Mexico (Rodriguez et al., 2008). The bay is shallow (3-m mean depth) and highly stratified through most of the year. The diurnal tides are microtidal (0- to 60-cm range) and have a tropic-equatorial cycle similar to the spring-neap cycle in semidiurnal systems. The large surface area of the bay (980 km^2) generates a sizable plume through Main Pass, delivering much of the needed estuarine nutrients to the “fertile crescent” of fisheries on the Mississippi Bight in the Gulf of Mexico (Dzwonkowski et al., 2017; Gunter, 1963). A 70-km long, 14-m deep shipping channel connects the Gulf of Mexico to the port of Mobile and continues (>3-m deep) up the Mobile Distributary and both rivers to the dams. These waterways flowing into Mobile Bay account for nearly half of all species extinctions in the United States during the twentieth century (U. S. Fish and Wildlife Service, 1998), and yet, descriptions of the delta's hydrology and geomorphology inland of the bay-head are limited to a few reports (e.g., O'Neil, 2007; Robinson & Powell, 1956; Smith, 1988) and requires further investigation.

4. Data and Methods

Long-term publicly available monitoring records were accessed for all data used in this study (Figure 1 and Tables S1 and S2). The 22 stations were labeled with the first letter representing the body of water (e.g., B:bay, D:delta, T:Tombigbee, and A:Alabama) followed by the distance inland from Main Pass along the longitudinal transect. A station not on the longitudinal axis was noted with an E (east, D96E). Data from D100 and stations landward were accessed from the USGS (waterdata.usgs.gov/nwis and by request from Alabama Water Science Center) while the stations seaward were accessed from NOAA (tidesandcurrents.noaa.gov and by request from the Center for Operational Oceanographic Products and Services) and the Alabama Real-Time Coastal Observing System (arcos.disl.org) with the exception of B8, which was from the USGS (Noble et al., 1992). Most stations had a sampling interval between 6 and 60 minutes. Longitudinal water level profiles of the largest recorded discharge events were extracted from the figures of O'Neil and Mettee (1982) and Robinson and Powell (1956) because the data used to produce them were incinerated (Job No. 77145 (1977)). Earth surface elevations were taken from USGS digital elevation models. Bathymetric elevations were from the Army Corps of Engineers eHydro Survey Data portal (geospatial-usace.opendata.arcgis.com/datasets/80a394bae6b547f1-b5788074261e11f1_0), including 112 hydrographic surveys (2012 to 2019) and a thalweg profile of the Alabama River (McComas & Copeland, 1996).

Total upstream discharge was derived from stations at the dams on the Tombigbee and Alabama Rivers, or nearby (27- and 9-km downstream, respectively) before dam closure (1960 and 1969, respectively). The two river discharges were highly correlated ($r^2 = 0.71$ for 89 overlapping years of mean daily flow) and were added together. The summed discharge was extrapolated for the entire delta watershed (Q_2) following the method of Gisen and Savenije (2015) and Waldon and Bryan (1999):

$$Q_2 = \frac{A_2}{A_1} * Q_1 \tag{4}$$

where Q_1, A_1, and A_2 are the summed discharge, station watershed area (provided by USGS), and delta watershed area (115,441 km^2; U. S. Geological Survey et al., 2019). All discharge herein refers to this calculated value. Water level stations with a datum were converted to NAVD88. A datum was linearly interpreted for D96E from the bulk average at upstream and downstream stations during low discharge (<300 $m^3\ s^{-1}$) following Coogan and Dzwonkowski (2018). To calculate thalweg elevations for L_b, high-resolution bathymetry was first bin averaged (20 m along channel and 5 m cross channel) before finding the maximum cross channel depth and applying a 15 km moving mean following Nittrouer et al. (2012). Since Bankhead et al. (2008) suggest upstream dams and dredging may have deepened the bed, the slopes of each thalweg profile were tested for significant changes (circles, Figure 2). Then, L_b was estimated by fitting a linear line to the thalweg profile, from the deep region (rkm 86; Figure 2) to the slope change on each river, and solving for the sea level intercept. Levee elevations were determined by using the lowest consistent crest for each river reach. Salinity measurements were taken at similar depths with bay sites measuring near the bed (0.5 m above the bottom) and channel sites measuring close to the mean depth of the bay (B22 and D52). Water current velocities were determined from acoustic Doppler current profilers orientated vertically (G-14 and B22) or horizontally (B47, D53, and D100) as well as a benthic acoustic stress sensor (B8). To minimize differences between collection methods, only bins between one quarter and one third of the water column depth were used, which included the index velocity of the horizontal sensors as determined by the source organization. The primarily flow axis was determined by the major tidal harmonic axis (K1 and O1) with t_tide (Pawlowicz et al., 2002). The average cross-sectional velocity at D100 was provided by the USGS using an index-velocity method accounting for tides (Ruhl & Simpson, 2005). While some data do not temporally overlap, all measurements could be referenced to discharge during a period without bathymetric changes in dredging or the construction of bridges or upstream dams. Specific details of data sources, length of records, and sensors used at each station is in the supporting information (Table S1).

The magnitude of water level, velocity, and salinity for a given discharge was computed as "rating curves." Data were first detided with a 40-hr Lanczos filter to remove the diurnal and higher frequency harmonics following Dzwonkowski et al. (2015). The low frequency harmonics (solar annual and solar semiannual) were the same order of magnitude as the water level rating curves at the bayhead. To remove these harmonics, their amplitudes and phases from the nearest tidal station outside of an estuary (provided by NOAA at

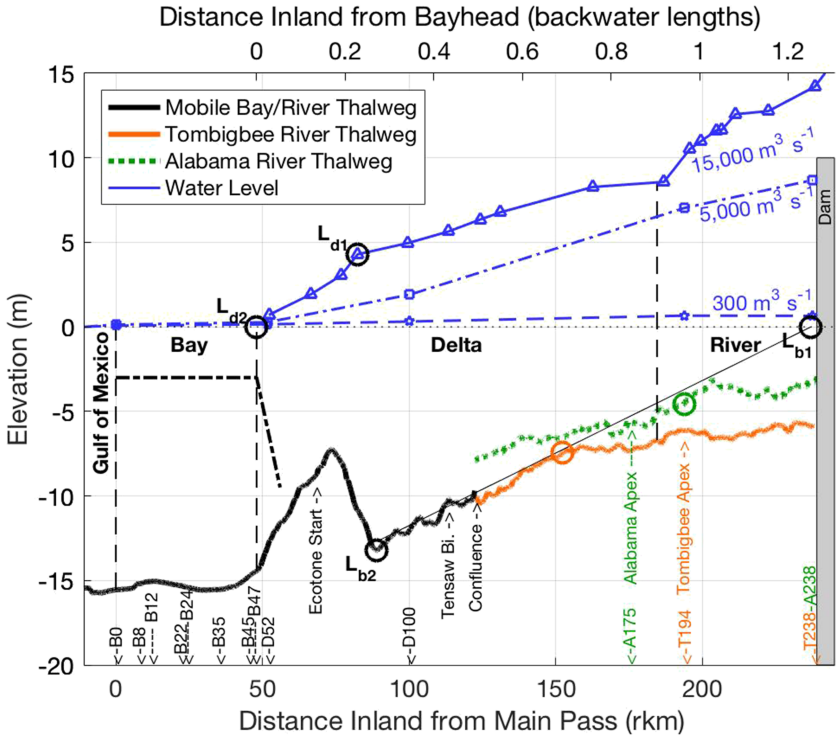

Figure 2. The longitudinal profile is showing water level (linearly interpreted) and thalweg elevation (15 km moving mean) from the Gulf of Mexico to the terminal Tombigbee dam. The thalweg elevation of the Alabama River is shown from the confluence to the terminal dam. A dredged channel for the Port of Mobile (seaward of rkm 56) was deeper than the rest of the bay and bayhead (black dash-dot line). To estimate the backwater length ($L_b = 151$ km), significant changes in the thalweg slope were detected on the Tombigbee and Alabama Rivers (circles). Station names reflect their distance inland from Main Pass (lower x axis).

Panama City Beach, FL 8729210) were used to calculate the low frequency tide following Pawlowicz et al. (2002). This tide was then subtracted from the water level measurements. At this point, water surface slopes were calculated as the change in water level divided by the distance between stations. Then, data were sorted by discharge with a mean lag (discussed below) and smoothed with a moving mean to form a "rating curve." To capture the environmental response to fluvial waves and not the intrusion rate, only salinity measurements during an increase in discharge were used. A loop water level-velocity rating curve was calculated for D100 with two velocity curves: one during rising water levels and the other during falling water levels. These curves helped explain results from the momentum balance calculation.

4.1. Momentum Balance of the Fluvial Wave

The momentum balance was calculated with equation (1) for the lower delta using measurements along the Mobile Distributary (D52 to D100). This reach was selected for its central location, simple geometry with a single channel and no major bifurcations, and long length of record (11 years). The dynamical analysis was conducted in the 2010 hydro year because it had the largest discharge events during the 11-year length of record when all needed measurements overlapped. In addition, this year included a typical low discharge summer and fall when the middle of the delta becomes tidal. In addition to the time series of the individual terms in equation (1), each term from the entire length of record was sorted by water level and ensemble averaged.

The time for a fluvial wave to propagate from the dams, acting as a control, to a downstream location was observed in the water level and velocity measurements (Figure 3). Celerity cannot be directly measured with observations so the mean travel time, or lag, between two points is calculated instead (Turner-Gillespie et al., 2003). The downstream lag time for each event was calculated from the peak discharge upstream to the peak water level and velocity at each site. Data was first low pass filtered with a Lanczos filter to reduce noise. The

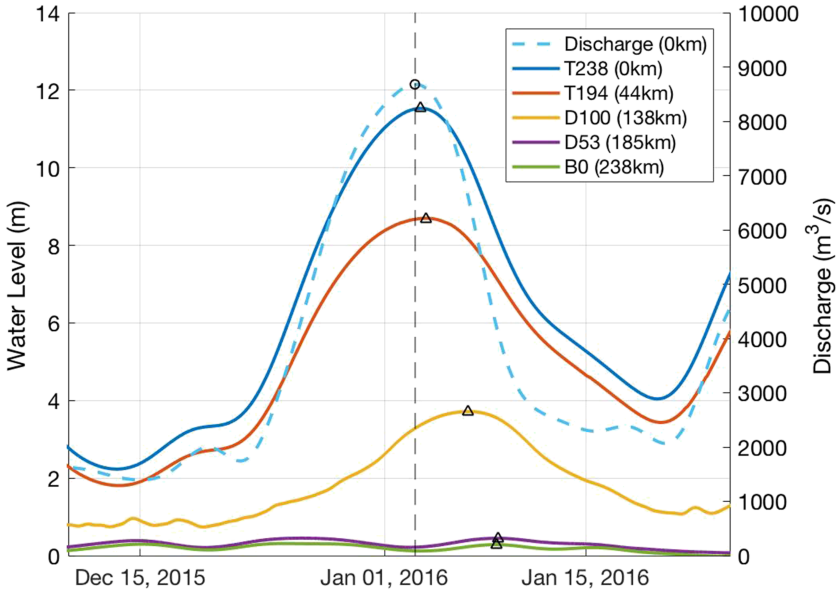

Figure 3. Time series of discharge and detided water level showing the propagation of a fluvial wave across the fluvial-marine transition in coastal Alabama. Peak water level (triangles) occurred after peak discharge (black dotted line) and at a later time downstream.

filtering window for discharge was 3 days to remove power peaking on the Alabama River. Water level and velocity had a 9-day window to account for the effects of wind, which have a dominant period of 2–8 days (Schroeder & Wiseman, 1986). Periods with strong winds exceeding twice the annual mean (4.1 ms^{-1}; Coogan & Dzwonkowski, 2018) were also removed. The remaining lags numbered between 58 and 651 for each station (except B8 with 18) and were ensemble averaged following the same method as the rating curves. A description of the confidence interval, phase, and wavelength calculations can be found in the supporting information.

5. Results

5.1. Role of Discharge on Estuarine Water Level, Velocity, and Salinity

Discharge entered the Alabama fluvial-marine transition at the terminal dams of the Tombigbee and Alabama Rivers with a relatively flat bed already below sea level (Figure 2). The thalweg slope steepened seaward to a deep region (averaging −12 to −13 m for rkm 85 to 100 and reaching −22 m at rkm 86) and then rapidly rose before reaching the port of Mobile where the ship channel made the thalweg profile much deeper than the bay. The lines used to determine the backwater length scale, from the deep region to significant slope changes, on the Tombigbee and Alabama had a good linear fit ($r = 0.94$ and 0.99, respectively) and similar slopes (8.9×10^{-5} and 8.3×10^{-5}). The estimated sea level intercepts of both rivers differed by only 1 km, averaging rkm 237 with $L_b = 151$ km. Scaling the delta by L_b (top x axis; Figure 2) showed the deepest location at $0.25L_b$ and the Tensaw Bifurcation at $0.43L_b$, almost identical to experimental locations of peak erosion and avulsion (Ganti et al., 2016a). The experimental location of peak deposition also corresponded to an area of high sinuosity on the Mobile Distributary and another bifurcation of the Tensaw Distributary. Along the backwater region, the levee elevation had a mean slope (-8.7×10^{-5}) similar to the thalweg, as expected in a balanced backwater system with variable flood discharge (Ganti et al., 2016b).

Mean discharge followed a common temperate trend with high flows in the spring and low flows in the summer and fall (Figure 4). The variability of flow around these mean conditions was high. Flow extremes ranged over 3 orders of magnitude (10^2–10^4 m^3 s^{-1}) with large and small events throughout the year. Clearly, the largest events occurred in the spring with maximum discharge values between 10,000 and 15,000 m^3 s^{-1}; however, the low flow periods of the summer and fall still experienced large events exceeding 4,000 m^3 s^{-1} in

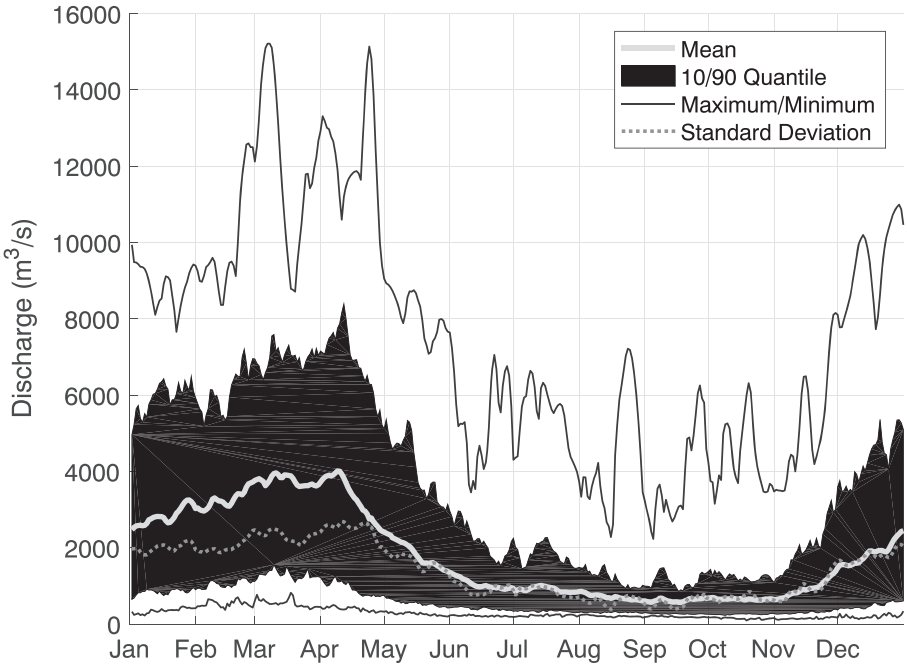

Figure 4. Annual discharge pattern of the Tom-Al Delta. Statistics were calculated from daily averaged data (1928–2017).

some cases. Similar to the mean conditions, there was a seasonal pattern in the standard deviation with larger values in the spring, but the low flow period did experience high variability relative to its mean with the standard deviations being nearly equal to the mean.

This temporal variability in the river discharge had varying responses downstream, which was characterized with ensemble averages of water level, water surface slope, surface velocity, and salinity under a broad range of conditions (Figure 5). In general, these measurements showed the largest sensitivity to discharge across the system, from the dams to the Gulf of Mexico, when flows were less than 2,000 $m^3\ s^{-1}$ (Figure 5). The ensemble averages in the water level, slopes, and velocity all showed notable increases with discharge between 0 and 2,000 $m^3\ s^{-1}$. Conversely, the salinity deceased rapidly with discharge over this same range.

There was also clear spatial structure in response to discharge at various regions in the system. The strongest water level response (Figure 5a) occurred at the furthest inland sites (A175, T194, T238, and A238) with less change at high discharge. In the downstream direction the response was weaker and more linear with increasing discharge. Interestingly, the Tombigbee River and the delta water levels were almost at the same as the Gulf of Mexico (T238 ~35 cm and D100 ~16 cm higher) at low river flow levels and showed no response to discharge until the flow exceeded 300 and 700 $m^3\ s^{-1}$, respectively. On the opposite end of the spectrum, when flow exceeded ~2,000 $m^3\ s^{-1}$, the water levels at the delta apices (T194 and A175) became the same and had a weaker response to discharge, indicating a transition from separate rivers to a single linked system. While less dramatic, the middle of the delta (D100) also had small noteworthy deviations from its linear relationship at approximately 2,000 and 5,000 $m^3\ s^{-1}$. At these flows the water level was 1.3 and 2 m, about the same elevation as the lowest local crevasses and the top of the local levees (2.1 m), respectively.

Changes in the water level were reflected in the water surface slope, where most of the system had slopes increasing linearly with discharge, except the upper delta (Figure 5b). The upper delta slopes increased the most during low discharge conditions and responded less as discharge increased until 5,000–6,000 $m^3\ s^{-1}$, above which there was no response to discharge. These different responses caused the longitudinal profile to change shape with discharge. The upper delta, compared to up and downstream of this region, usually had a steeper slope but became more gradual for high discharge events (>8,000 $m^3\ s^{-1}$). These trends observed in our data continue to the highest recorded discharge (15,000 $m^3\ s^{-1}$; Figure 5b, right).

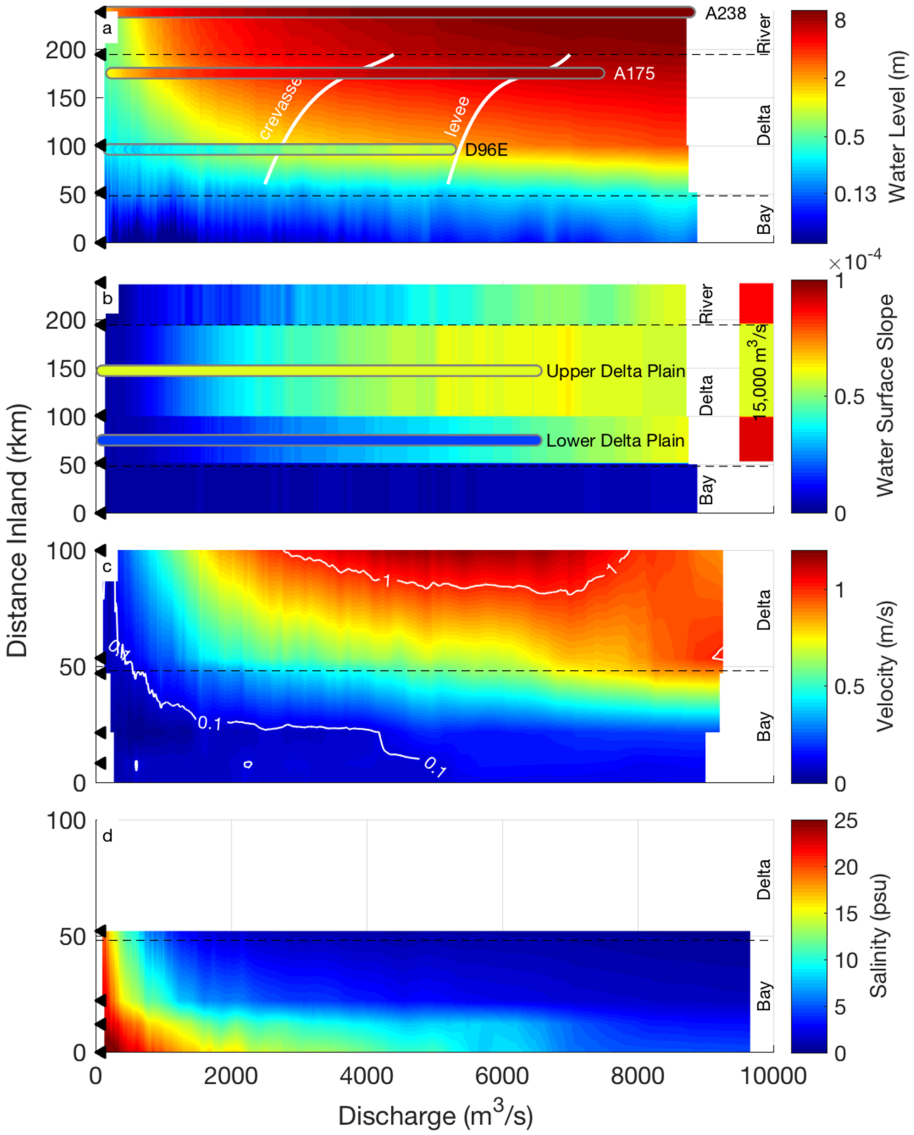

Figure 5. Longitudinal conditions by discharge for (a) water level, (b) water surface slope, (c) surface velocity, and (d) salinity. The response to discharge at a given location is seen by looking at a horizontal section of the plot while the longitudinal response in the system at a specific discharge is captured with a vertical section. Stations along the Tombigbee River-Mobile Distributary-Mobile Bay transect are noted on the y-axis (triangles) and regions (i.e., river, delta, and bay) are delineated with a dashed line. Additional (a) water levels and (b) the delta plain slope are shown as elongated horizontal ovals (outlined in gray) at their respective distances inland. (a) The approximate discharge water levels that exceed the lower crevasse and levee elevations in the delta are shown with curved white lines. (b) Water surface slopes at maximum measured discharge (~15,000 $m^3\ s^{-1}$) are on the right.

The water surface slope controlled the barotropic pressure gradient and the velocity of freshwater. Like the water level, the seaward velocity increased with discharge was greatest inland and usually decreased seaward until reaching the bay (Figure 5c). The bay and gulf velocity had a weak response to discharge with a noticeable increase for $Q > 5{,}000\ m^3\ s^{-1}$ (white line). The bay head's velocity increased linearly with one prominent inflection at 1,500–2,000 $m^3\ s^{-1}$ and surpassed the delta velocity at high flow (>8,000 $m^3\ s^{-1}$). This velocity in the middle of the delta (D100) reflected the upstream water surface slopes with a decreasing response to discharge until plateauing at 5,000 $m^3\ s^{-1}$ (white line). Above 6,500 $m^3\ s^{-1}$, the velocity interestingly slowed down as discharge increased (further discussed in section 5.2).

The seaward velocity and associated freshwater transport modulated the salt and freshened the bay as discharge increased (Figure 5d). Salinity observations were highest at Main Pass (D0) where estuarine water

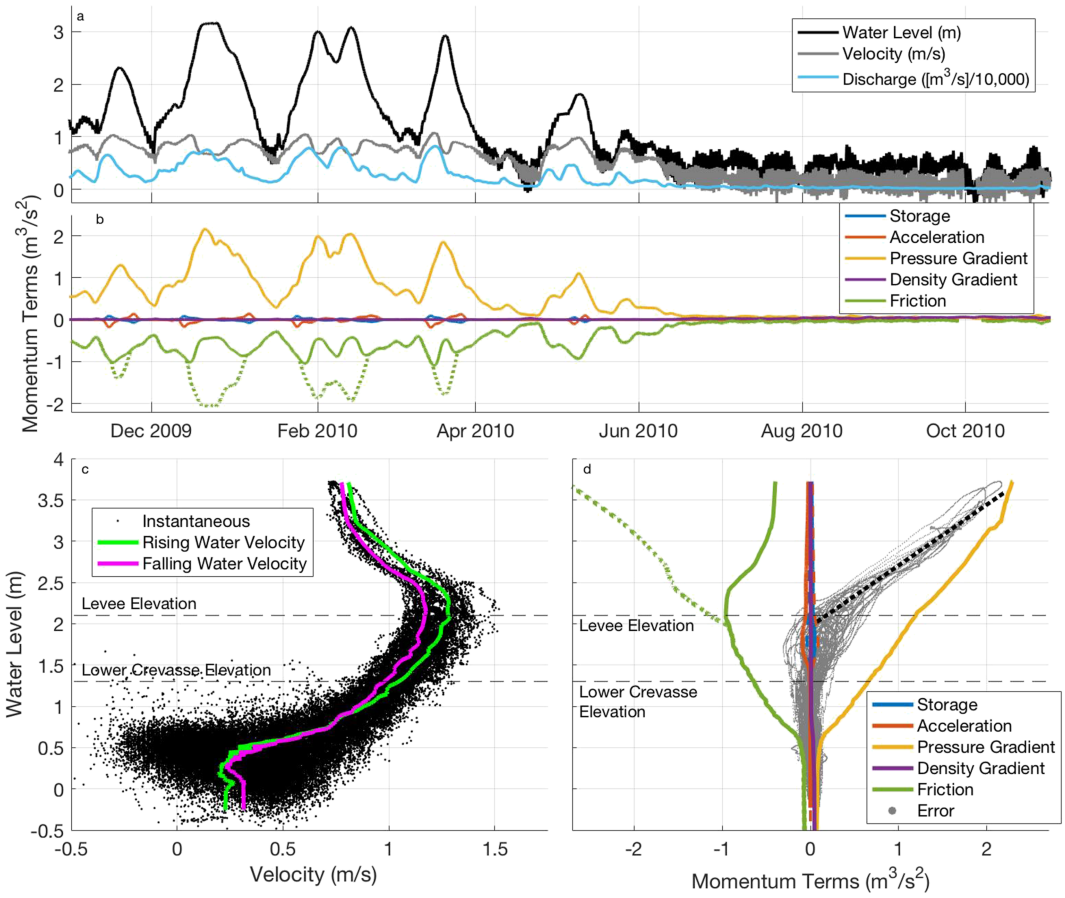

Figure 6. (a, c) Hydraulic conditions and (b, d) momentum balances at D100 as (a, b) a time series and (c, d) by water level. To capture water level dynamics in c and d, instantaneous (dots) and ensemble averaged (lines) measurements are shown. (d) Storage and acceleration terms were separated for rising (solid) and falling (dashed) water levels. Above the levee, the pressure gradient continued to increase but the friction decreased creating error that linearly increased with water level (b, d; dotted lines).

exchanged with the Gulf of Mexico and gradually decreased landward until the bay head (D52). While there are no long-term salinity records in the delta, previous work by Robinson and Powell (1956) measured salinity decreasing landward with measurable concentrations at D100. Salinity at the bay head flushed at low discharge and approached zero at 1,500–2,000 $m^3\ s^{-1}$. For higher discharge conditions the salinity at all stations responded less to an increase in discharge with one exception. Pass aux Herons (B12) salinity dropped much more when discharge exceeded 5,500 $m^3\ s^{-1}$ causing it to nearly reach the salinity of Main Pass (D0). In summary, observations of water level, water surface slope, velocity, and salinity over a broad range of discharge levels revealed that flows of 2,000, 5,000, and 8,000 $m^3\ s^{-1}$ were critical points where system responses changed.

5.2. Momentum Balances

The nonlinear water level, velocity, and salinity response to discharge was examined with momentum balances for the lower delta (Figure 6). Time series of the terms in the momentum balance are shown in conjunction with the parameters used to characterize the system, that is, water level, slope, and velocity (Figures 5a and 5b). The two dominant terms in the momentum balance were pressure gradient and friction, with the other terms often several orders of magnitude smaller. The evolution of these terms over the course of a discharge event shows a consistent and notable shift in the system dynamics. As the discharge increased, the pressure gradient also increased and was initially balanced by friction as a diffusive wave (Figure 6b). As the pressure gradient term peaked, the friction term decreased. As the pressure gradient began to decease after the peak in discharge, the friction term then increased again returning to a diffusion wave balance. Interestingly, at these transition points the smaller acceleration and storage terms peaked and balance

each other due to a large change in cross-sectional area. During low discharge periods, the momentum drastically decreased and all the terms ranged within 1 or 2 orders of magnitude.

In order to further explore the observed dynamical shift during high discharge events, the system velocity and dynamics were characterized at different water level stages (Figures 6c and 6d). Instantaneous measurements from 11 years at D100 revealed a consistent velocity relationship with the rising and falling of water level (Figure 6c). Above a small rise in water level (>0.7–1 m), the reversing tide (ranging 0 to 90 cm s^{-1}) became unidirectional and then ceased as the water continued to rise. The rising water level had a stronger velocity than the falling water level (i.e., the difference between the pink and green lines) with the largest difference of 14 cm s^{-1} at bankfull discharge. The lines form a wide loop rating curve and indicate unsteady-flow conditions with acceleration and error that can be seen in the momentum balance (Figure 6d). The velocity peaked when the water level reached the levee elevation (2.1 m; i.e., bankfull discharge) and decreased as the water level became higher. As the water level dropped after peaking, the velocity increased until bankfull discharge and then decreased.

When the momentum balances were ensemble averaged by water level, they more clearly depict the changes observed in the time series (Figure 6d). As the water levels rose and the tides waned, the pressure gradient and friction terms began to increase with the water level (>60 cm) and balanced each other with small errors above the lower crevasse elevations (1.3 m). When the water level exceeded the levee, the pressure gradient term continued to increase but the friction term decreased and resulted in large errors in the balance that were of similar magnitude to the pressure gradient term. These errors suggest a major component of friction was not accounted for, increasing linearly with water level at 1.4 $m^3 s^{-2}$ per meter (dotted line). Even though the storage term included the entire width of the flood plain, it remained small regardless of water level. The changes in the momentum balance observed during high discharge events in 2010 and at transition points in the delta topography were reflected in the fluvial wave celerity.

5.3. Fluvial Flood Wave Propagation

The fluvial flood wave celerity through coastal Alabama's rivers, delta, and bay was observed with water level and velocity measurements to have a nonlinear relationship and at times inverse relationship to discharge. Figure 3 captures the largest flooding event when all water level measurements were available. In a downstream direction, the water level generally peaked at a later time and at a lower elevation. This demonstrates the propagation and changing shape of a fluvial wave as it traveled from the source river through the delta and bay to the mouth of the system.

Combining a wide range of events captured dramatically different responses to an event's size in the upstream and downstream regions (Figure 7). As the size of discharge events increased, the lag times decreased in the rivers and main distributary of the delta (D100). As flow exceeded ~2,000 $m^3 s^{-1}$ the delta and bay lag times increased with discharge until ~5,000 $m^3 s^{-1}$ after which the lag times were consistent regardless of discharge. Even though the bay results were noisy, the trends followed the significant changes upstream in the delta (e.g., D100). The smaller Tensaw Distributary (D96E) had the same lag time as the bay at low discharge and transitioned at higher flows to a lag time that was nearly consistent with the larger Mobile Distributary (D100). Similarly, the lag times observed with velocity showed a decrease with discharge during low flow events and an increase in lag time with higher flow events while not changing when discharge peaked above 5,000 $m^3 s^{-1}$. The bay measurements were noisier than the delta but followed similar trends.

The water level and velocity lag times were compared at D100 to evaluate how the character of the fluvial flood wave changed depending on the discharge event (Figure 7d). The velocity lag time was significantly less than the water level lag time for the entire discharge range. However, when discharge was low and flow was in the channel, the flood wave traveled up to 2 times faster in the velocity signal than the water level signal, making them strongly out of phase (~70°, using equation (S1)). Larger discharge events lasted for longer periods and the water level lag time increased more relative to the velocity lag time. This caused the fluvial flood wave to become more in phase, reaching ~20°. At 600, 1,000 and 2,000 $m^3 s^{-1}$, wavelengths across the upper delta were approximately 350, 530, and 1,060 km, respectively. Results at the bayhead were similar to D100 with significantly different water level and velocity lag times and larger events delivering waves more in phase (not shown).

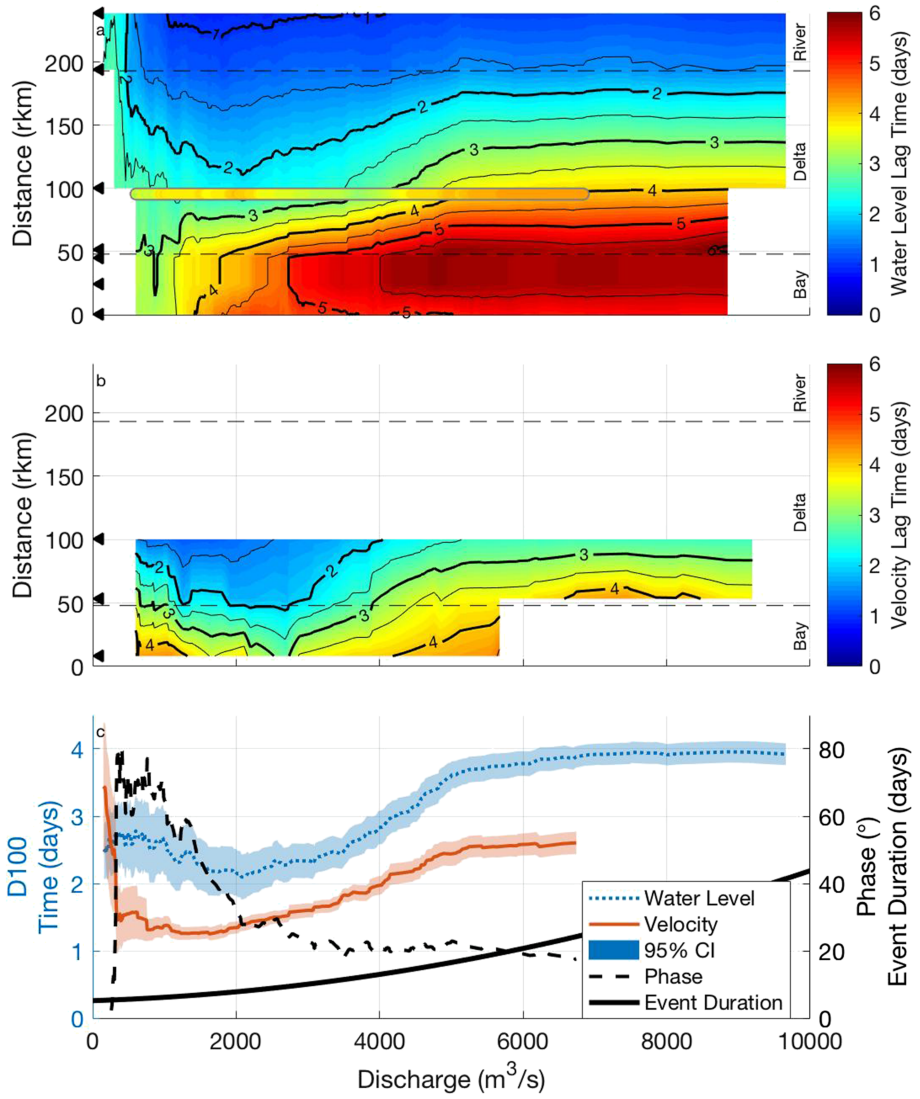

Figure 7. Fluvial wave lag times from peak discharge at upstream dams to downstream measurements of peak (a) water level and (b) velocity are shown for the Tombigbee River-Mobile Distributary-Mobile Bay longitudinal transect. Additional lag times for D96E, on the Tensaw Distributary, are shown as an elongated horizontal oval (outlined in gray) at its respective distance inland (96 rkm). The response to discharge at a given location is seen by looking at a horizontal section of the plot while the longitudinal response in the system at a specific discharge is captured with a vertical section. (c) The water level and velocity lag times for D100 with a 95% confidence interval.

Viewing the lag times longitudinally more clearly shows how celerity varied with distance downstream and event size (Figure 8). The water level and velocity measurements had very similar celerities across the lower delta (26 and 30 cm s^{-1}, respectively, for overbank events) with a ~1- to 2-day longer lag time in the water level, approximately the same lag time observed at the dams where discharge was measured (T238 and A238). Across most of the delta, discharge events confined to the channel (<2,000 m^3 s^{-1}; circles and stars) propagated faster as the event size increased, reaching 91 cm s^{-1}, 3 times faster than large events with overbank flow (5,000–8,000 m^3 s^{-1}; triangles). Further seaward, events moved faster across the lower delta and bay. The small in-channel events traveled at 440 cm s^{-1}, an order of magnitude faster than the lower delta while overbanking and close to the speed of a tidal wave. Surprisingly, the celerity of the velocity measurement appeared slower across the bay, giving water level and velocity the same lag time in the lower bay near Main Pass. Estimations of celerity ($c = 1.5u$, slope of red lines) can be compared to the slope of the lines upstream and downstream from a station. Estimated celerity for large in-channel events were

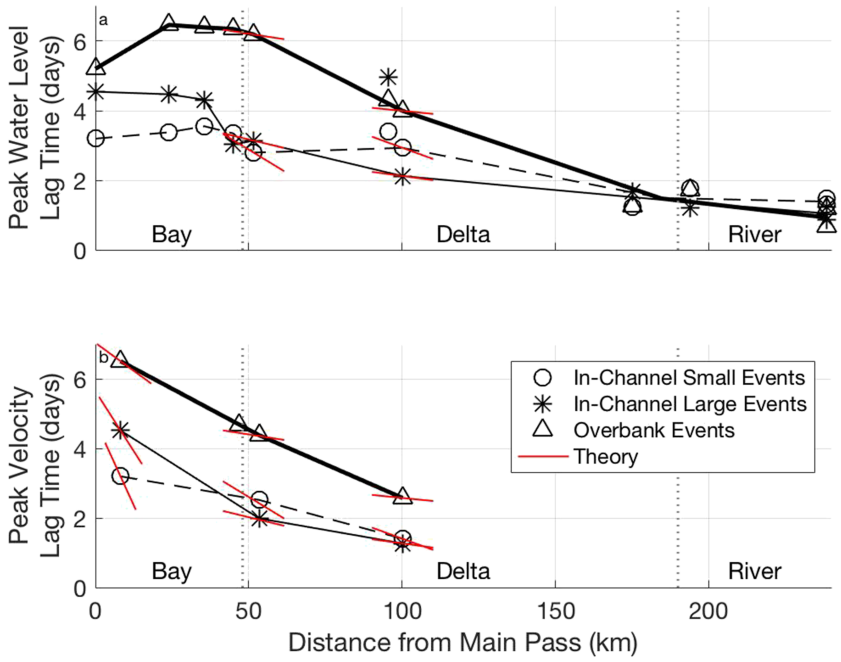

Figure 8. A longitudinal view of the mean lag time from peak discharge to (a) peak water level and (b) peak velocity for discharge events grouped by conditions in the delta: small events confined to the channel (600–1,000 $m^3\ s^{-1}$; circles), larger events confined to the channel (1,500–2,000 $m^3\ s^{-1}$; stars), and events causing overbank flow (5,000–8,000 $m^3\ s^{-1}$; triangles). The slope of the lines can be interpreted as the celerity of the wave where near vertical lines are slow and horizontal lines are fast. The celerity of $c = 1.5u$ is shown (slope of red lines) over symbols where velocity measurements were available. Lines show averaged lag times at the dams (T238 and A238) and the delta apices (T194 and A175). This was not done for the delta where the larger Mobile Distributary (D100) was dynamically different than the Tensaw Distributary (D96E).

close to the waver level and velocity measurements (6% and 27% faster, respectively), but for overbank flow, the estimation was 4 times the observed celerity. This was likely due to the mean channel velocity not capturing the slower flow on the floodplain. At Main Pass, flow was much slower and did not appear to predict the celerity either, except during large events that flushed most of the bay. Overall, wave celerity had spatial variability and changed at 2,000 and 5,000 $m^3\ s^{-1}$ like the rating curves and momentum balance.

Table 1
Summary of Discharge Conditions and Fluvial Flood Wave Dynamics

Discharge	Q < 300–600	600 < Q < 2,000	2,000 < Q < 5,000	5,000 < Q
Delta Flow	Tidal	Channel Flow	Crevasse Flooding	Overbank Flow
Backwater Profile	Backwater (M1)	Backwater (M1)	Backwater (M1)	Drawdown (M2)
Occurrence (%)	32	39	21	8
Recurrence (per year)	--	--	6.9	2.9
Fluvial Flood Wave Type (Response to Discharge)				
Rivers	Dynamic[a]	Diffusive	Diffusive	Diffusive
Celerity	(no change)	(increase)	(no change)	(no change)
Attenuation	(no change[a])	(decrease[a])	(no change[a])	(no change[a])
Delta	Dynamic	Diffusive	Diffusive	Diffusive
Celerity	(no change)	(increase)	(decrease)	(no change)
Attenuation	(no change[a])	(decrease[a])	(increase[a])	(decrease[a])
Bay	Dynamic	Dynamic	Dynamic	Dynamic
Celerity	(no change)	(decrease)	(decrease)	(no change)
Attenuation	(no change[a])	(increase[a])	(increase[a])	(unknown)

[a]Estimated from environmental conditions

6. Discussion

6.1. Hydrodynamic Conditions of the Backwater-Estuarine Environment

The magnitude, celerity, and phasing (Figures 5a and 5c, 8, and 7c, respectively) of fluvial flood waves were captured for discharge events ranging 3 orders of magnitude in a coastal backwater-estuarine environment. The shallow water equations compliment the wave observations and highlight the role of topography and friction on wave celerity and attenuation (figure 6). The range of discharge created four distinct hydrodynamic conditions in the backwater-estuarine environment of the delta, each modulating the wave propagation and discharge differently (table 1): nonfluvial, channel flow, crevasses flooding, and overbank flow.

6.1.1. The Backwater-Estuarine Environment

All low-lying coastal rivers have a backwater-estuarine environment that strongly influences the fluvial-marine transition by scaling the geomorphology, hydrodynamics, and ecology with L_b (Ganti et al., 2016a; Gugliotta et al., 2017; Nittrouer et al., 2012; Tsai, 2005). This is observed in mesotidal environments (e.g., Gugliotta & Saito, 2019), and this study demonstrates the scaling also applies to microtidal environments. The L_b scaling relationship in the Tom-Al Delta would have been poor, with a long L_b, if the thalweg near the dams was used to calculate L_b (Figure 2). This suggests the low upstream bed elevations are out of morphodynamic balance and may have incised. Incising is commonly caused by dams and dredging and has been observed in similar systems such as the lower Columbia and Hudson Rivers (Helaire et al., 2019; Ralston & Geyer, 2017). Models show the Columbia River historically flooded large areas, like the modern Tom-Al Delta, and are now separated from river channels or require a larger discharge to flood (Helaire et al., 2019). Channel incision can decrease fluvial wave attenuation and increase celerity (Sholtes & Doyle, 2011), changes that may have altered the dynamics of the Tombigbee and Alabama Rivers upstream of slope changes. The calculated L_b scaling of the Alabama fluvial-marine transition still closely reflected theory, experiments, and field observations. This, combined with discharge ranging over 3 orders of magnitude to represent a wide range of hydrodynamic conditions, suggests the findings of this study are widely applicable to other systems.

6.1.2. Nonfluvial, Channel Flow, and Crevasse Flooding

The lowest discharge conditions were non-fluvial with a small water surface slope of 1.5×10^{-6} (D0 to T238) that would be expected from residual tidal circulation in a lagoon without any discharge (Table 1 and Figure 9b; Li & O'Donnell, 2005). The marine environment reached far inland with tides propagating to the dams (both 238 rkm inland) and salt intruding to the delta, averaging as high as 20 psu at the bayhead. The confined channel flow (600–2,000 $m^3\ s^{-1}$) was highly sensitive to discharge and overwhelmed the tide so it could not reverse the flow in the delta (i.e., tidal river) making the bayhead fresh. These were the most common conditions (39% of the time; Table 1). As discharge rose in the delta, channel flow exchanged with the floodplain through natural crevasses in the levees (i.e., crevasse flooding) 6.9 times per year on average (2,000–5,000 $m^3\ s^{-1}$; Figure 9c). The data indicated water escaping through crevasses created sharp changes in the water level, velocity, and salinity response to discharge (Figure 5) even though the momentum had small changes in the combined storage and error (Figure 6d). These small momentum changes were larger than at bankfull conditions likely due to flooding through crevasses, a process that diffuses the sudden effects of overbanking in other systems such as the Mississippi, Ob, and Altamaha Rivers (Mertes, 1997).

6.1.3. Overbank Flow and Floodplain Dynamics

High discharge conditions ($Q >$ 5,000 $m^3\ s^{-1}$) in the delta were dominated by flow over the floodplain because levees were submerged and flood basins freely connected to each other and the channels (Table 1 and Figure 9d). All water surface slopes increased linearly with discharge except across the upper delta, where there was no slope change once overbank conditions were reached (Figure 5b). The water level was less sensitive to high discharge at the bayhead where friction is expected to be less (via slower flow velocity and less vegetation). This created a drawdown profile (M2) when the lower delta's water surface slope became steeper than the upper delta and caused flow to accelerate seaward (Figure 5c). Historical water level profiles with higher spatial resolution show the slope transition was more dramatic (4.1 to 11.8×10^{-5} for 1961 flood) and occurred near the railroad bridge over the Mobile Distributary (rkm 82). Interestingly, this region begins the transition, or ecotone, from forested tidal wetlands landward to oligohaline marshes seaward (U. S. Fish and Wildlife Service, 2019; Figures 1 and 2). Because friction is higher from rigid trees than submerged flexible grasses (Allison et al., 2013), it suggests the vegetation caused the upper delta water level to rise more and create normal flow conditions (i.e., bed and water surface slope are the same) over the delta

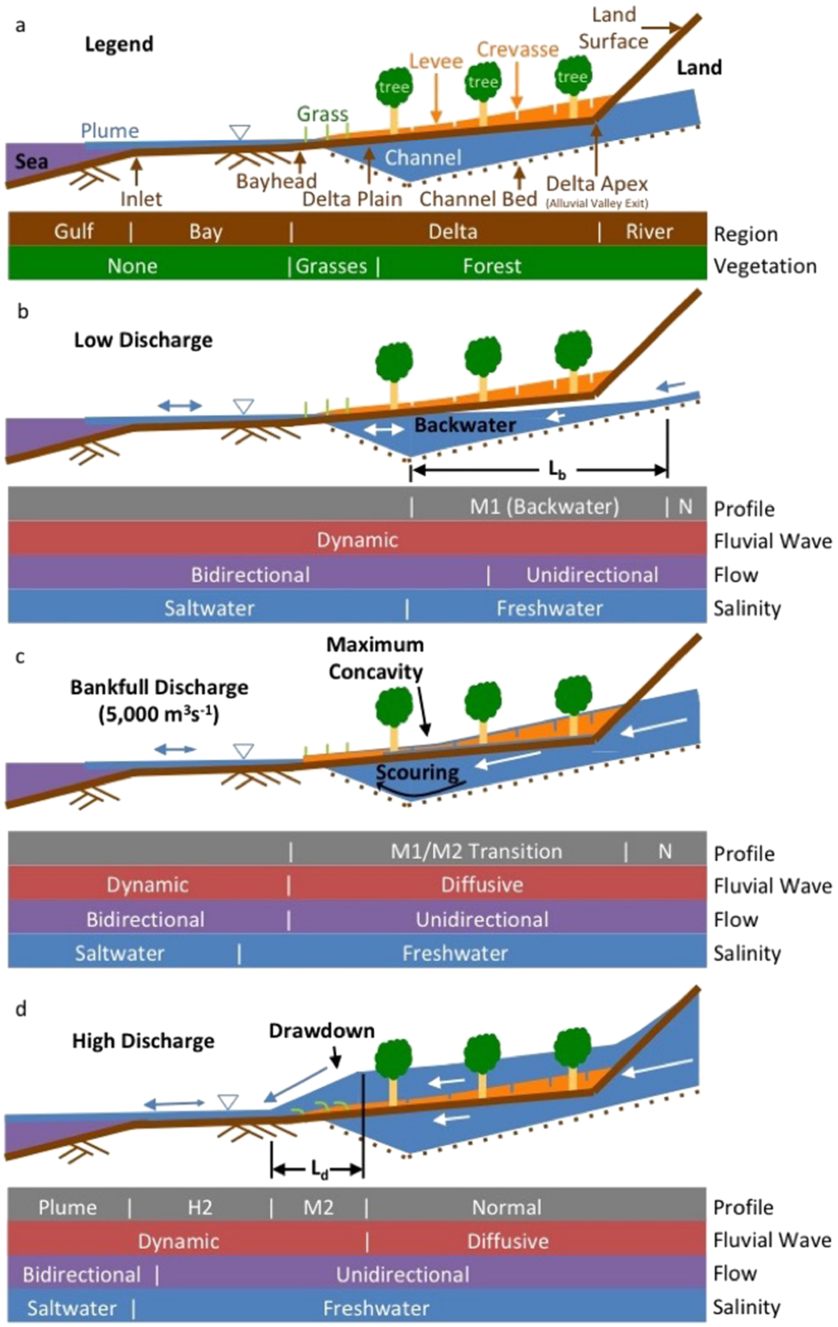

Figure 9. A cartoon cross-section depicting the longitudinal dynamics of coastal Alabama under (b) low, (c) bankfull, and (d) high discharge conditions. Low discharge created a long backwater environment. At bankfull discharge maximum concavity was reached and scoured the bed creating a deep location inland. Bankfull discharge also marks the M1-M2 transition because the dominant bed switches from the channel to the delta plain. At high discharge the forest's friction slows water and creates a convex drawdown profile due to acceleration over the lower friction of the grasses and bay. The blue triangle shows the water surface.

plain. As this transition occurred, the velocity at D100 became less sensitive to discharge until decreasing at overbank conditions, suggesting the forested channel banks generated enough shear to slow the flow in the channel (Figures 5c and 6c). This process is observed on the River Severn with direct measurements in the channel and floodplain as well as captured in models (Knight & Shiono, 1996). The trees also explain the unaccounted friction in the momentum equation during overbank conditions (Figure 6d) and appear to impact the drawdown.

6.2. Backwater-Drawdown Transition

The surface water slope and bed slope in the upper delta suggest this region was a backwater during the entire length of record (i.e., bed slope > surface water slope); however, the dominant bottom surface during overbank flow was the delta plain (Figure 9d). By switching the bed slope at bankfull discharge, the upper delta switched from a backwater to near normal flow and the lower delta switched to drawdown. This demonstrates the M1-M2 transition can occur at bankfull discharge as suggested by Lamb et al.'s (2012) model of the Mississippi River and may be typical of other systems. It also suggests the floodplain slope may be more useful than the bed slope for hydraulic calculations (e.g., M1-M2) during overbank conditions.

The analytical solution for drawdown length ($L_d = 0.5L_b$; Lamb et al., 2012) indicates the Tom-Al drawdown should be 76 km, twice the observed length (Figure 2). The observed drawdown length of 34 kms was only $L_d = 0.23L_b$ and suggests the ecotone may have caused the drawdown to be shorter and closer to the bay (Figure 9d). This also steepened and intensified drawdown, reaching a slope 2.9 times larger than the upper delta during peak discharge (Figure 2). This may be common as drawdown profiles on the Apalachicola River, Florida (Leonardi et al., 2015), also show the slope transition occurring just landward of the forest-marsh ecotone.

The location of drawdown seaward of the commonly observed deep region in a coastal bed profile was surprising and indicates drawdown did not scour it as suggested by studies using prismatic conditions (Figure 9d; e.g., Ganti et al., 2016a; Chatanantavet et al., 2012). Scouring in streams is most effective at bankfull discharge and increases with surface water slope concavity (i.e., difference of upstream and downstream slope; Copeland et al., 2005; Blom et al., 2016). This agrees with the results showing maximum concavity in the water surface slope at the deep region (D100) during bankfull discharge when the velocity also peaked (Figures 2, 5b, 5c, and 9c). This suggests fluvial forces in the Tom-Al Delta scoured the backwater bed profile during the M1-M2 transition at bankfull discharge and not at drawdown. Water surface concavity occurs in all coastal rivers due to the sea level being flat and usually increases with flow. This may explain the widespread observations of the backwater bed profile in a range of systems from macrotidal environments without drawdown (e.g., Gugliotta & Saito, 2019) to freshwater coasts like the Laurentian Great Lakes (Lane, 1957).

6.3. Fluvial Flood Waves

Fluvial waves were observed propagating from inland dams through a deltaic-estuarine environment to the Gulf of Mexico. To our knowledge, these are the first reported observations of discharge propagating as a fluvial wave through an estuary and indicate fluvial waves do not stop in rivers. Instead, they likely transitioned from diffusive to dynamic waves and are modulated by the environment they propagate through, critically impacting the flushing of the estuary and exchange with the shelf.

6.3.1. Transition From Diffusive to Dynamic Waves

Our results indicate fluvial wave celerity and attenuation increased in a downstream direction closely reflecting the theory of waves propagating along a flattening slope (e.g., Ponce & Simons, 1977). Data suggest k^* increased in a seaward direction, making wave types transition from diffusive waves to dynamic waves (red box; Figure 9c). Explaining this with the momentum terms, the dynamic wave formed due to a downstream decrease in pressure gradient slowing the flow of water, subsequently decreasing friction within 2 orders of magnitude of the acceleration term. Previous observations of celerity have ranged from 25 cm s^{-1} for a diffusive wave (Brakenridge et al., 1998) to 1,000 cm s^{-1} for a dynamic wave (Allen et al., 2018; Sriwongsitanon et al., 1998). This agrees well with the wide range of observed values in the fluvial-marine transition of Alabama, suggesting the slower inland waves were diffusive and transitioned to dynamic waves in the delta or bay where they traveled an order of magnitude faster and quickly attenuated (Figure 8).

Our results suggest this diffusive-dynamic transition was not fixed and moved seaward for larger events (Table 1). The pressure gradient and friction were small at D100 during low flow making the acceleration term relatively important and suggests waves were dynamic. The transition at D100 to diffusive waves was observed when the pressure gradient and friction terms increased and balanced each other as the water level rose (Figure 6). These observations with water level and velocity measurements provide a unique opportunity to see changes in the phasing of fluvial waves (Figure 7c). In this coastal backwater, the horizontal component (i.e., velocity) peaked more than a day before the vertical component (i.e., water level), an

order of magnitude longer than low lying inland rivers (Dottori et al., 2009). For small events, the time gap was almost a quarter of the wave period causing the dynamic waves to be out of phase and propagate quickly. This had an almost uniform rise and fall in the water level across the system like flow routing in a reservoir or a standing tidal wave. As the slope increased and formed a diffusive wave, it had a gradient to propagate along that decreased the lag time of the vertical component more than the horizontal component (Figure 8). This combined with an increase in the event duration (i.e., period) made the wave nearly in phase (equation (S1); Figure 7c). In phase diffusive waves are commonly assumed in fluvial dynamics, allowing water level-measurements to account for both vertical and horizontal wave components. Identifying where and at what discharge the diffusive-dynamic transition occurs is critical for understanding fluvial waves in coastal environments.

Since wave types form a spectrum, the distribution of momentum can be simply estimated by solving for k^*, and in backwater environments, k^* can be approximated with equation (3). Our L_b and λ were the same order of magnitude (estimated k^* values of 0.43, 0.29, and 0.14 for peak discharge events at 600, 1,000, and 2,000 m^3 s^{-1}, respectively) and suggest the backwater may have caused the waves to be dynamic. Analytical solutions (see Tsai, 2005; using an observed Fr~0.1 at D100) suggest a wave is diffusive in backwater conditions when $k^* < 1/3$ or dynamic when k*~1/3–2. Waves in the Tom-Al Delta were approximately three times the backwater length (i.e., k*~1/3) when peak event discharge was 600–1,000 m^3 s^{-1}, suggesting larger discharge events had diffusive waves and the smallest discharge events had dynamic waves. The discharge of this transition was the same as observed with the momentum balance (Figure 6), when fluvial waves became more in phase, and when flow transitioned from tidal to unidirectional channel flow (Table 1). The results suggest fluvial waves propagate to the sea as diffusive waves in unidirectional flow where fluvial forces are dominant (i.e., tidal river) and transition to dynamic waves in bidirectional flow where tidal currents become stronger than fluvial currents (Figure 9).

6.3.2. Environmental Impacts on Wave Celerity

The celerity had two primary responses to the environment it propagated through: (1) an increase in discharge magnitude increased the surface slope leading to faster wave celerity and (2) an increase in cross-sectional area slowed the wave celerity. The steepening of the surface slope forms diffusive waves and increases the velocity, causing larger discharge events to propagate faster with a shorter downstream lag time. This was captured in Figures 7 and 8 for small events when flow was confined to the channel and is a common assumption in rivers with limited flooding (e.g., Muskingum-Cunge Method).

Wave celerity decreases if the cross-sectional area increases more than discharge and is simply explained through the Kleitz-Seddon law of $c = dx/dt = dQ/dA$, obtained by rearranging the conservation of mass (Kleitz, 1877; Seddon, 1900). The law is consistent with the data where area greatly increased by widening into the delta floodplains and may have happened by freshwater filling the water column in the bay. In the Tom-Al, a small rise in water level allowed flow through the levees (via crevasses) to the floodplains to rapidly expand the cross-sectional area and decrease the wave celerity. The celerity stopped decreasing at bankfull discharge because the change in area stopped rapidly increasing when water covered the entire floodplain to the edges of the delta's valley (~5,000 m^3 s^{-1}; Figure 7a).

Downstream, the bay water is stratified like most estuaries, with seaward freshwater flow on the surface and a salty landward flow along the bottom during low river discharge conditions. Stratification reduces friction in the surface layer allowing tidal waves to propagate faster (Burchard et al., 2018). The two-layer flow structure can be disrupted by large discharge events filling the water column and destratifying the system. Noble et al. (1996) captures the disruption in Mobile Bay at D8 as the discharge increases above 3,000 m^3 s^{-1}, where the seaward flowing cross-sectional area significantly increases. Instead of celerity slowing from an increase in water level increasing the cross-sectional area, like observed in the delta, the stratified bay may have decreased wave celerity by deepening the surface layer and pushing the salt wedge seaward. This would have also increased friction at the same time. The bayhead flushing was at a lower discharge than D8 (Figure 5d) and may explain why during low discharge events the celerity in the bay slowed as the event size increased while the celerity in the delta became faster (Figure 7a). This difference ceased as salt flushed (figure 5d) and the bay became a destratified extension of the fluvial environment. Other estuarine process may also be impacting fluvial wave celerity. For example, during high flow events water level consistently peaked at Main Pass before the rest of the bay (Figures 3 and 8a). This is likely associated with the hydrodynamics of

Main Pass, which may generate supercritical flow (Noble et al., 1996), a process that lowers the water level as flow increases (Poggioli & Horner-Devine, 2018).

6.3.3. Fluvial Wave Attenuation and Estuarine Exchange

While fluvial waves have not been previously reported in coastal environments, fluctuations in celerity and attenuation from surface slope and floodplains have been observed and modeled in rivers (Anderson et al., 2006; Turner-Gillespie et al., 2003; Wolff & Burges, 1994). These studies show the same processes slowing a fluvial wave usually attenuate peak discharge. They also demonstrate attenuation from flooding with the peak of a wave propagating down a channel while loosing water to the floodplain. This floodplain water flows slower due to higher friction and may return to the channel once the wave peak has past. This decreases downstream peak water level and discharge while increasing the duration of an event. These studies used floodplain to channel width ratios as large as 5:1, but in coastal environments like the Tom-Al Delta where the ratio is 30:1, these effects are expected to be more dramatic in estuarine environments.

Fluvial waves attenuating with cross-sectional area was clearly observed in this study with the river elevations raising 2 orders of magnitude more than the broad bay for the same size events (Figure 5a). While discharge is difficult to measure at the coast, the affects and attenuation of discharge can still be seen. The results show when the delta flooding caused wave celerity to decrease as event sizes increased (2,000–5,000 $m^3\ s^{-1}$), downstream in the bay, velocity and flushing stopped increasing with discharge (Figures 5c and 5d). This suggests the peak discharge reaching the bay was only a fraction of the upstream measurement, consistent with flooding through the crevasses reducing river discharge into the bay.

Large discharge events in rivers can have less attenuation when flooding reaches the valley walls and the water level begins to rise faster again like confined channel flow conditions. This causes the downstream peak discharge to more closely reflect an upstream peak discharge (Turner-Gillespie et al., 2003; Woltemade & Potter, 1994; Sholtes & Doyle, 2011). In coastal Alabama, water completely spread over the floodplain at bankfull discharge (5,000 $m^3\ s^{-1}$). During overbank flow in the delta, the bay velocity and flushing increased with discharge events similar to flow confined to the channel ($Q < 2{,}000\ m^3\ s^{-1}$; Table 1). These overbank conditions have a fundamentally different response to relative flooding levels than the flooding through crevasses, highlighting the fact that smaller flooding events attenuate more than large flooding events.

Large changes in attenuation made the inland discharge measurements unrepresentative for discharge in the bay and may explain why some discharges values have been observed marking a critical shift in the controlling factors that determine estuarine and coastal circulation. Models not accounting for flooding in the delta show a smooth decrease in the flushing time of Mobile Bay (ranging 4-131 days) with discharge (Du et al., 2018; Webb & Marr, 2016). However, observations by Abston et al. (1987) and Dinnel et al. (1990) show the Mobile Bay plume size switches from correlating with the tidal range to discharge when $Q > 4{,}500\ m^3\ s^{-1}$ from upstream measurements (~4,800 $m^3\ s^{-1}$ after watershed conversion; equation (4)). This threshold occurs when attenuation of the fluvial flood wave decreases in the delta (i.e., flood plain filling has been achieved) allowing discharge to pass more easily through the delta. At this time, the upstream measurement becomes more representative of actual discharge influencing the bay. This threshold shift in system response to discharge suggests the flooding dynamics inland of the bay play a significant role in increasing the transport of estuarine water, sediments, and nutrients further on the shelf.

6.4. Fluvial Waves in Other Coastal Environments

Our results indicate fluvial waves in the fluvial-marine transition are almost identical to marine waves in propagation and interaction with the local bathymetry. Long waves from tides and storm surge accelerate (decelerate) from convergence (divergence) and attenuate as the water rises over a tidal flat (Jay, 1991) similarly to fluvial wave flooding. Tides can also become highly asymmetric due to friction with faster rising water levels than falling and result in waves that reflect hydrographs and loop-rating curves (Airy, 1841; Dronkers, 1986). Fluvial waves usually propagate in one direction (primary wave) but crevasses and sloughs (e.g., Tonlé Sap River, Cambodia) can flood and ebb like a low frequency tide (Smith, 1988; Kummu et al., 2014).

One distinction between fluvial and marine waves is clear. On the wave type spectrum, fluvial waves span the small k^* (diffusive) side of the celerity inflection point (Ponce, 1989). Marine waves have very mild slopes giving them a large k^* and indicate their momentum is similar to gravity waves, as observed in the open ocean where frictional dissipation is low (Hendershott, 1973). While fluvial and marine waves can both be dynamic

waves, theory indicates the closer one approaches the middle of the dynamic k^* range the more it will attenuate and limits them from having the same k^*. As one approaches from land and the other from the sea, they share a common space of attenuation in the fluvial-marine transition. Beyond momentum there may not be any dynamical difference between these long waves and is an interesting question for future research.

This study indicates fluvial waves are estuarine long waves, like storm surge and tides, and should be used as part of coastal hydrodynamics for flood preparation, navigation, and research. The magnitude and timing of a discharge event in estuaries is dynamic and only first order estimates can be reached by using traditional estuarine methods of an upstream magnitude and a constant lag time. Newer methods of estimating coastal discharge (e.g., Hoitink et al., 2009; Moftakhari et al., 2013) have significant limitations and could be improved with or replaced by fluvial waves for more precise temporal and spatial estimates. Results suggest subtidal discharge could be simply and accurately estimated in tidal rivers with flow routing techniques accounting for diffusive momentum. In contrast to Alabama's microtidal environment, larger tides form wider channels that decrease fluvial flooding and overbank flow (Hoitink et al., 2017). They can also push salt, ecotones, and tidal rivers further inland (Gugliotta et al., 2017). This could decrease the frequency, magnitude, or length of drawdown and push the dynamic-diffusive transition further inland than observed in this study. However, these differences may be muted since convergence length (Dronkers, 2017; Leuven et al., 2018), delta area, subaerial delta gradient, and distributary channels (Syvitski & Saito, 2007) correlate more with discharge than marine forces.

Backwater environments and fluvial wave propagation are nonstationary with temporal modulations and long-term changes that need to be anticipated for managers and future research to understand compound events. Seasonality of temperate forests modifies friction (Järvelä, 2002) and may cause summer (winter) conditions to shorten (extend) L_d, intensify (decrease) drawdown effects, and attenuate fluvial waves more (less). Furthermore, sea level rise is increasing tidal amplitude and should increase L_d while pushing the dynamic-diffusive transition inland. These tides are also bringing saltwater inland and pushing ecotones with it (Ensign & Noe, 2018). This potential extension of the ecotone would be expected to decrease drawdown effects and fluvial wave attenuation.

Climate change is also expected to modify the ecotone. Mangrove trees are expanding poleward and replacing temperate oligohaline marshes, which would be expected to increase friction in the ecotone. As a result, this transition should decrease L_d, intensify drawdown, and attenuate fluvial waves. Interestingly, Alabama is predicted to have one of the largest mangrove invasions in the Northern Gulf of Mexico (Doyle et al., 2010), which provide the potential for significant modification to fluvial wave dynamics observed in this study. Additional affects of direct human intervention by modifying the geometry or sediment transport with levees, dredging, or dams on backwater environments and fluvial waves in coastal areas also requires further attention.

7. Conclusion

Fluvial flood waves were captured propagating from rivers into the Gulf of Mexico through a backwater deltaic-estuarine environment with measurements of water level and velocity from 22 stations over multiple years. In particular, this study found geometry, vegetation, and marine forces modulated the timing and magnitude of the fluvial waves. System geometry scaled with L_b as prescribed (e.g., Ganti et al., 2016a), indicating a representative system and that these findings should have broad applicability to other systems. The backwater to drawdown transition, a process that dramatically changes the hydrodynamics and geomorphology of a system, was modeled on the Mississippi River at bankfull discharge (Lamb et al., 2012), and this study provides observational support of those findings. Interestingly, results suggest drawdown was intensified and had a shorter length (L_d) than theory due to the forest-marsh ecotone on the delta plain likely changing the frictional environment. Additionally, the momentum balance suggests high friction at overbank flow caused the channel velocity to slow down. While this process has been rarely observed in a natural setting, in part due to a lack of measurements, this work indicates it may be common in coastal backwaters and could change how a system scales with L_b.

Observations of fluvial waves propagating through a coastal backwater-estuarine environment reflected theory indicating waves change from diffusive waves (friction-pressure gradient balance) to dynamic waves

(friction-pressure gradient-acceleration balance) as bed slope decreases. This made fluvial waves propagate faster and attenuate more. Observations supported approximating wave type with k^*, using L_b and λ in a backwater, as an alternative to solving a momentum balance. The location of the diffusive-dynamic transition moved downstream for larger events with the transition from unidirectional to bidirectional flow. Instead of celerity and magnitude consistently increasing with the size of discharge events, as commonly assumed in coastal environments, an important finding in this study was that flooding caused fluvial waves to slow and attenuate due to the larger cross-sectional area. This flooding modulated estuarine flushing and estuarine-shelf exchange.

To capture these dynamics in coastal areas, an interdisciplinary approach from fluvial hydrology (i.e., flow routing) and estuarine circulation is needed. Current methods (e.g., Saint Venant equations) used in observational studies cannot alone capture complex friction from vegetation (e.g., riparian zone) or two-layer flow. Hydrodynamic models will require grids to extend inland to discharge stations and have a high resolution of elevation to capture exchange with floodplains while precisely representing overbank flow. Model friction will need to account for the vertical changes in vegetation while still capturing estuarine circulation (i.e., baroclinic, tidal, and wind). Direct observations of timing between stations with long length of records, liked used in this study, provide the best celerity estimates but are not numerous and can be noisy, which present an inherent limitation for precisely measuring discharge at the coast. Lastly, the impacts of fluvial and fluvial-marine compound flooding could be reduced if managers limit channelization of coastal rivers, increase the area and friction (e.g., trees) of inland floodplains, and can predict the precise timing as well as the magnitude of fluvial events by tracking the propagation of fluvial waves into their coastal environment.

Acknowledgments
This research was made possible in part by a grant from the Gulf of Mexico Research Initiative (CONCORDE) and in part by the NOAA Restore Science Program (NA17NOS4510101). Data are publicly available through the Gulf of Mexico Research Initiative Information & Data Cooperative (GRIIDC) at https://data.gulfresearchinitiative.org (doi: 10.7266/6tdw4xsv), USGS at https://waterdata.usgs.gov/nwis, NOAA at tidesandcurrents.noaa.gov and https://cmist.noaa.gov, the Alabama Coastal Real-Time Observing System (ACROS) at https://arcos.disl.org, and the Army Corps of Engineers eHydro Survey at geospatial-usace.opendata.arcgis.com/datasets/80a394bae6b547f1b5788074261e11f1_0. Direct links to datasets are provided in the Supporting Information. Some of the ACROS data were collected by the Tech Support Group at the Dauphin Island Sea Lab, including Kyle Weis, Roxanne Robertson, Alan Gunter, Mike Dardeau, Grant Lockridge, Hunter King, Y. Hintz, Laura Linn, and Renee Collini. We would like to thank Kelly Dorgan for her advising, Joseph Wallace for explaining the collection of USGS data, Christopher Esposito for early suggestions and references, and Arnoldo Valle-Levinson for figure suggestions.

References

Abston, J. R., S. P. Dinnel, W. W. Schroeder, and A. W. Shultz (1987), Coastal sediment plume morphology and its relationship to environmental forcing: Main Pass, Mobile Bay, Alabama, Coastal Sediments 87: proceedings of a Specialty Conference on Advances in Understanding of Coastal Sediment Processes, New Orleans, Louisiana.

Airy, G. B. (1841). *Tides and waves*. London: Encycl. Metrop.

Allen, G. H., David, C. H., Andreadis, K. M., Hossain, F., & Famiglietti, J. S. (2018). Global estimates of river flow wave travel times and implications for low-latency satellite data. *Geophysical Research Letters*, *45*, 7551–7560. https://doi.org/10.1029/2018GL077914

Allison, M. A., Kolker, A., & Meselhe, E. (2013). Water and sediment dynamics through the wetlands and coastal water bodies of large river deltaic plains, in *Biogeochemical dynamics at major river-coastal interfaces*, pp. 21–54.

American Association of Port Authorities (2015). U.S. port rankings by Cargo Volume 2016, Chart.

Anderson, B. G., Rutherfurd, I. D., & Western, A. W. (2006). An analysis of the influence of riparian vegetation on the propagation of flood waves. *Environmental Modeling & Software*, *21*(9), 1290–1296. https://doi.org/10.1016/j.envsoft.2005.04.027

Bankhead, N., Simon, A., & Klimetz, D. (2008). *Analysis of Streambank Erosion Along the Lower Tombigbee River*. Alabama: U.S Department of Agriculture- Agriculture Research Service.

Blom, A., Viparelli, E., & Chavarrías, V. (2016). The graded alluvial river: Profile concavity and downstream fining. *Geophysical Research Letters*, *43*, 6285–6293. https://doi.org/10.1002/2016GL068898

Brakenridge, G. R., Tracy, B. T., & Knox, J. C. (1998). Orbital SAR remote sensing of a river flood wave. *International Journal of Remote Sensing*, *19*(7), 1439–1445. https://doi.org/10.1080/014311698215559

Burchard, H., Schuttelaars, H. M., & Ralston, D. K. (2018). Sediment trapping in estuaries. *Annual Review of Marine Science*, *10*(1), 371–395. https://doi.org/10.1146/annurev-marine-010816-060535

Chatanantavet, P., Lamb, M. P., & Nittrouer, J. A. (2012). Backwater controls of avulsion location on deltas. *Geophysical Research Letters*, *39*, L01402. https://doi.org/10.1029/2011GL050197

Chow, T. V. (1959). *Open-channel hydraulics* (Vol. 1). New York: McGraw-Hill.

Coogan, J., & Dzwonkowski, B. (2018). Observations of wind forcing effects on estuary length and salinity flux in a river-dominated, microtidal estuary, Mobile Bay, Alabama. *Journal of Physical Oceanography*, *48*(8), 1787–1802. https://doi.org/10.1175/JPO-D-17-0249.1

Copeland, R., Soar, P., & Thorne, C. (2005). Channel-Forming Discharge and Hydraulic Geometry Width Predictors in Meandering Sand-Bed Rivers. *Impacts of Global Climate Change*. https://doi.org/10.1061/40792(173)568

Cunge, J. A. (1969). On The Subject Of A Flood Propagation Computation Method (Musklngum Method). *Journal of Hydraulic Research*, *7*(2), 205–230. https://doi.org/10.1080/00221686909500264

Dinnel, S. P., Schroeder, W. W., & Wiseman, W. J. Jr. (1990). Estuarine-shelf exchange using Landsat images of discharge plumes. *Journal of Coastal Research*, *6*(4), 789–799.

Dottori, F., Martina, M. L. V., & Todini, E. (2009). A dynamic rating curve approach to indirect discharge measurement. *Hydrology and Earth System Sciences*, *13*(6), 847–863. https://doi.org/10.5194/hess-13-847-2009

Doyle, T. W., Krauss, K. W., Conner, W. H., & From, A. S. (2010). Predicting the retreat and migration of tidal forests along the northern Gulf of Mexico under sea-level rise. *Forest Ecology and Management*, *259*(4), 770–777. https://doi.org/10.1016/j.foreco.2009.10.023

Dronkers, J. (1986). Tidal asymmetry and estuarine morphology. *Netherlands Journal of Sea Research*, *20*(2/3), 117–131.

Dronkers, J. J. (1964). Tidal computations in rivers and coastal waters, in Tidal computations in Rivers and Coastal Waters, North-Holland, Amsterdam.

Dronkers, J. J. (2017). Convergence of estuarine channels. *Continental Shelf Research*, *144*, 120–133. https://doi.org/10.1016/j.csr.2017.06.012

Du, J., Park, K., Shen, J., Dzwonkowski, B., Yu, X., & Yoon, B. I. (2018). Role of baroclinic processes on flushing characteristics in a highly stratified estuarine system, Mobile Bay, Alabama. *Journal of Geophysical Research: Oceans*, *123*, 4518–4537. https://doi.org/10.1029/2018JC013855

Dzwonkowski, B., Fournier, S., Reager, J. T., Milroy, S., Park, K., Shiller, A. M., et al. (2018). Tracking sea surface salinity and dissolved oxygen on a river-influenced, seasonally stratified shelf, Mississippi Bight, northern Gulf of Mexico. *Continental Shelf Research*, *169*, 25–33. https://doi.org/10.1016/j.csr.2018.09.009

Dzwonkowski, B., Greer, A. T., Briseño-Avena, C., Krause, J. W., Soto, I. M., Hernandez, F. J., et al. (2017). Estuarine influence on biogeochemical properties of the Alabama shelf during the fall season. *Continental Shelf Research*, *140*, 96–109. https://doi.org/10.1016/j.csr.2017.05.001

Dzwonkowski, B., Park, K., & Collini, R. (2015). The coupled estuarine-shelf response of a river-dominated system during the transition from low to high discharge. *Journal of Geophysical Research: Oceans*, *120*, 6145–6163. https://doi.org/10.1002/2015JC010714

Ensign, S. H., & Noe, G. B. (2018). Tidal extension and sea-level rise: Recommendations for a research agenda. *Frontiers in Ecology and the Environment*, *16*(1), 37–43. https://doi.org/10.1002/fee.1745

Ensign, S. H., Noe, G. B., & Hupp, C. R. (2014). Linking channel hydrology with riparian wetland accretion in tidal rivers. *Journal of Geophysical Research: Earth Surface*, *119*, 28–44. https://doi.org/10.1002/2013JF002737

Fernandes, A. M., Törnqvist, T. E., Straub, K. M., & Mohrig, D. (2016). Connecting the backwater hydraulics of coastal rivers to fluvio-deltaic sedimentology and stratigraphy. *Geology*, *44*(12), 979–982. https://doi.org/10.1130/G37965.1

Ganti, V., Chadwick, A. J., Hassenruck-Gudipati, H. J., Fuller, B. M., & Lamb, M. P. (2016a). Experimental river delta size set by multiple floods and backwater hydrodynamics. *Science Advances*, *2*(5), e1501768–e1501768. https://doi.org/10.1126/sciadv.1501768

Ganti, V., Chadwick, A. J., Hassenruck-Gudipati, H. J., & Lamb, M. P. (2016b). Avulsion cycles and their stratigraphic signature on an experimental backwater-controlled delta. *Journal of Geophysical Research: Earth Surface*, *121*, 1651–1675. https://doi.org/10.1002/2016JF003915

Ghanbari, M., Arabi, M., Obeysekera, J., & Sweet, W. (2019). A coherent statistical model for coastal flood frequency analysis under nonstationary sea level conditions. *Earth's Future*, *7*(2), 162–177. https://doi.org/10.1029/2018EF001089

Gisen, J. I. A., & Savenije, H. H. G. (2015). Estimating bankfull discharge and depth in ungauged estuaries. *Water Resources Research*, *51*, 2298–2316. https://doi.org/10.1002/2014WR016227

Greene, D. L. Jr., Rodriguez, A. B., & Anderson, J. B. (2007). Seaward-branching coastal-plain and piedmont incised-valley systems through multiple sea-level cycles: Late quaternary examples from Mobile Bay and Mississippi Sound, U.S.A. *Journal of Sedimentary Research*, *77*(2), 139–158. https://doi.org/10.2110/jsr.2007.016

Gugliotta, M., & Saito, Y. (2019). Matching trends in channel width, sinuosity, and depth along the fluvial to marine transition zone of tide-dominated river deltas: The need for a revision of depositional and hydraulic models. *Earth-Science Reviews*, *191*, 93–113. https://doi.org/10.1016/j.earscirev.2019.02.002

Gugliotta, M., Saito, Y., Van Lap, N., Ta, T. K. O., Nakashima, R., Tamura, T., et al. (2017). Process regime, salinity, morphological, and sedimentary trends along the fluvial to marine transition zone of the mixed-energy Mekong River delta, Vietnam. *Continental Shelf Research*, *147*, 7–26. https://doi.org/10.1016/j.csr.2017.03.001

Gunter, G. (1963). The fertile fisheries crescent. *Journal of Mississippi Academy of Science*, *9*, 286–290.

Hamill, L. (1983). Some observations on the time of travel of waves in the River Skerne, England, and the effect of aquatic vegetation. *Journal of Hydrology*, *66*(1-4), 291–304. https://doi.org/10.1016/0022-1694(83)90191-9

Hartley, A. J., Weissmann, G. S., & Scuderi, L. (2016). Controls on the apex location of large deltas. *Journal of the Geological Society*, *1–4*. https://doi.org/10.6084/m9.figshare.c.3469770

Helaire, L. T., Talke, S. A., Jay, D. A., & Mahedy, D. (2019). Historical changes in lower Columbia river and estuary floods: A numerical study. *Journal of Geophysical Research: Oceans*, *124*, 7926–7946. https://doi.org/10.1029/2019JC015055

Hendershott, M. C. (1973). Long waves and ocean tides. *Eos, Transactions American Geophysical Union*, *2*(10), 292–341.

Hoitink, A. J. F., Buschman, F. A., & Vermeulen, B. (2009). Continuous measurements of discharge from a horizontal acoustic Doppler current profiler in a tidal river. *Water Resources Research*, *45*, W11406. https://doi.org/10.1029/2009WR007791

Hoitink, A. J. F., & Jay, D. A. (2016). Tidal river dynamics: Implications for deltas. *Reviews of Geophysics*, *54*, 240–272. https://doi.org/10.1002/2015RG000507

Hoitink, A. J. F., Wang, Z. B., Vermeulen, B., Huismans, Y., & Kästner, K. (2017). Tidal controls on river delta morphology. *Nature Geoscience*, *10*(9), 637–645. https://doi.org/10.1038/ngeo3000

Hopkinson, C. S., & Vallino, J. J. (1995). The relationships among man's activities in watersheds and estuaries: A model of runoff effects on patterns of estuarine community metabolism. *Estuaries*, *18*(4), 598–621. https://doi.org/10.2307/1352380

Järvelä, J. (2002). Flow resistance of flexible and stiff vegetation: A flume study with natural plants. *Journal of Hydrology*, *269*(1-2), 44–54. https://doi.org/10.1016/s0022-1694(02)00193-2

Jay, D. A. (1991). Green's law revisited: Tidal long-wave propagation in channels with strong topography. *Journal of Geophysical Research*, *96*(C11), 20,585–20,598. https://doi.org/10.1029/91JC01633

Jay, D. A., Borde, A. B., & Diefenderfer, H. L. (2016). Tidal-fluvial and estuarine processes in the lower Columbia River: II. Water Level Models, floodplain wetland inundation, and system zones. *Estuaries and Coasts*, *39*(5), 1299–1324. https://doi.org/10.1007/s12237-016-0082-4

Job No. 77145 (1977). Request for authority to dispose of records, from Department of the Army, National Archives and Records Service, Washington, D. C.

Kästner, K., Hoitink, A. J. F., Torfs, P. J. J. F., Vermeulen, B., Ningsih, N. S., & Pramulya, M. (2018). Prerequisites for accurate monitoring of river discharge based on fixed-location velocity measurements. *Water Resources Research*, *54*, 1058–1076. https://doi.org/10.1002/2017WR020990

Kästner, K., Hoitink, A. J. F., Vermeulen, B., Geertsema, T. J., & Ningsih, N. S. (2017). Distributary channels in the fluvial to tidal transition zone. *Journal of Geophysical Research: Earth Surface*, *122*, 696–710. https://doi.org/10.1002/2016JF004075

Kidd, K. R., Copenheaver, C. A., & Aust, W. M. (2015). Sediment accretion rates and radial growth in natural levee and backswamp riparian forests in southwestern Alabama, USA. *Forest Ecology and Management*, *358*(C), 272–280. https://doi.org/10.1016/j.foreco.2015.09.025

Kleitz, M. (1877). Note sur la theorie du mouvement non permanent des liquides et sur application a la propagation des crues des rivieres (Note on the theory of unsteady flow of liquids and on application to flood propagation in rivers). *Annales des ponts et chaussees*, *16*, 133–196.

Knight, D. W., & Shiono, K. (1996). River channel and floodplain hydraulics. In M. G. Anderson, D. E. Walling, & P. D. Bates (Eds.), *Floodplain Processes* (pp. 139–181). New York: John Wiley & Sons Ltd.

Kummu, M., Tes, S., Yin, S., Adamson, P., Józsa, J., Koponen, J., et al. (2014). Water balance analysis for the Tonle Sap Lake-floodplain system. *Hydrological Processes*, *28*(4), 1722–1733. https://doi.org/10.1002/hyp.9718

Lamb, M. P., Nittrouer, J. A., Mohrig, D., & Shaw, J. (2012). Backwater and river plume controls on scour upstream of river mouths: Implications for fluvio-deltaic morphodynamics. *Journal of Geophysical Research*, *117*, F01002. https://doi.org/10.1029/2011JF002079

Lane, E. W. (1957). A study of the shape of channels formed by natural streams flowing in erodible material, United States Army Corps of Engineers.

Leonardi, N., Kolker, A. S., & Fagherazzi, S. (2015). Interplay between river discharge and tides in a delta distributary. *Advances in Water Resources*, *80*, 69–78. https://doi.org/10.1016/j.advwatres.2015.03.005

Leuven, J. R. F. W., van Maanen, B., Lexmond, B. R., van der Hoek, B. V., Spruijt, M. J., & Kleinhans, M. G. (2018). Dimensions of fluvial-tidal meanders: Are they disproportionally large? *Geology*, *1–4*. https://doi.org/10.1130/G45144.1

Li, C., & O'Donnell, J. (2005). The Effect of Channel Length on the Residual Circulation in Tidally Dominated Channels. *Journal of Physical Oceanography*, *35*(10), 1826–1840. https://doi.org/10.1175/jpo2804.1

Lighthill, M. J., & Whitham, G. B. (1955). On kinematic waves. I. Flood movement in long rivers. *Proceedings of the Royal Society A: Mathematical, Physical and Engineering Sciences*, *229*(1178), 281–316.

Lininger, K. B., & Latrubesse, E. M. (2016). Flooding hydrology and peak discharge attenuation along the middle Araguaia River in central Brazil. *Catena*, *143*, 90–101. https://doi.org/10.1016/j.catena.2016.03.043

Losada, M. A., Díez-Minguito, M., & Reyes-Merlo, M. Á. (2017). Tidal-fluvial interaction in the Guadalquivir River Estuary: Spatial and frequency-dependent response of currents and water levels. *Journal of Geophysical Research: Oceans*, *122*, 847–865. https://doi.org/10.1002/2016JC011984

Mancini, E. A., Mink, R. M., Tew, B. H., Kopaska-Merkel, D. C., & Mann, S. D. (1991). Upper Jurassic smackover oil plays in Alabama, Mississippi and the Florida Panhandle. *Gulf Coast Association of Geological Societies Transactions*, *41*, 475–480.

Matte, P., Secretan, Y., & Morin, J. (2018). Reconstruction of tidal discharges in the St. Lawrence fluvial estuary: The method of cubature revisited. *Journal of Geophysical Research: Oceans*, *123*, 5500–5524. https://doi.org/10.1029/2018JC013834

McComas, D. N., & R. Copeland (1996). Sediment impact assessment for navigation channel maintenance, Alabama River, Alabama and Apalachicola River, Florida, US Army Corp of Engineers.

Mertes, L. A. K. (1997). Documentation and significance of the perirheic zone on inundated floodplains. *Water Resources Research*, *33*(7), 1749–1762. https://doi.org/10.1029/97wr00658

Moftakhari, H. R., AghaKouchak, A., Sanders, B. F., Allaire, M., & Mattheus, C. R. (2018). What is nuisance flooding? Defining and monitoring an emerging challenge. *Water Resources Research*, *54*, 4218–4227. https://doi.org/10.1029/2018WR022828

Moftakhari, H. R., Jay, D. A., & Talke, S. (2016). Estimating river discharge using multiple-tide gauges distributed along a channel. *Journal of Geophysical Research: Oceans*, *121*, 2078–2097. https://doi.org/10.1002/2015JC010983

Moftakhari, H. R., Jay, D. A., Talke, S., Kukulka, T., & Bromirski, P. D. (2013). A novel approach to flow estimation in tidal rivers. *Water Resources Research*, *49*, 4817–4832. https://doi.org/10.1002/wrcr.20363

Nittrouer, J. A., Shaw, J., Lamb, M. P., & Mohrig, D. (2012). Spatial and temporal trends for water-flow velocity and bed-material sediment transport in the lower Mississippi River. *Geological Society of America Bulletin*, *124*(3-4), 400–414. https://doi.org/10.1130/B30497.1

Noble, M.A., Gelfanbaum, G., Strahle, W. J., Martini, M. A., & Ferriera, J. T. (1992). Oceanographic measurements—Mobile Bay, Alabama, 1990-1992, United States Geological Survey data release. https://stellwagen.er.usgs.gov/mobile_bay.html.

Noble, M. A., Schroeder, W. W., Wiseman, W. J. Jr., Ryan, H. F., & Gelfenbaum, G. (1996). Subtidal circulation patterns in a shallow, highly stratified estuary: Mobile Bay, Alabama. *Journal of Geophysical Research*. https://doi.org/10.1029/96JC02506/full

O'Neil, P. E. (2007), A synoptic water-quality survey in the upper Mobile-Tensaw River Delta, 2005-2007, Geological Survey of Alabama.

O'Neil, P. E., & Mettee, M. F. (Eds.) (1982). Alabama coastal region ecological characterization. Volume 2. A synthesis of environmental data, United States Fish and Wildlife Service, Office of Biological Services.

Pawlowicz, R., Beardsley, B., & Lentz, S. J. (2002). Classical tidal harmonic analysis including error estimates in MATLAB using T_TIDE. *Computers & Geosciences*, *28*(8), 929–937. https://doi.org/10.1016/S0098-3004(02)00013-4

Poggioli, A. R., & Horner-Devine, A. R. (2018). Two-layer hydraulics at the river-ocean interface. *Journal of Fluid Mechanics*, *856*, 633–672. https://doi.org/10.1017/jfm.2018.688

Ponce, V. M. (1989). *Engineering hydrology*. Englewood Cliffs, NJ: Prentice Hall.

Ponce, V. M., Li, R.-M., & Simons, D. B. (1978). Applicability of kinematic and diffusion models. *Journal of the Hydraulics Division*, *353–360*.

Ponce, V. M., & Simons, D. B. (1977). Shallow wave propagation in open channel flow. *Journal of the Hydraulics Division*, *1461–1477*.

Ralston, D. K., & Geyer, W. R. (2017). Sediment transport time scales and trapping efficiency in a tidal river. *Journal of Geophysical Research: Earth Surface*, *122*, 2042–2063. https://doi.org/10.1002/2017JF004337

Robinson, W. H., & Powell, W. J. (1956). Water resources of the Mobile area, Alabama, United States Department of the Interior.

Rodriguez, A. B., Greene, D. L. Jr., Anderson, J. B., & Simms, A. R. (2008). Response of Mobile Bay and eastern Mississippi Sound, Alabama, to changes in sediment accommodation and accumulation. *Geological Society of America Special Papers*, *443*, 13–29.

Ruhl, C. A., & M. R. Simpson (2005). Computation of discharge using the index-velocity method in tidally affected areas, United States Geological Society.

Schroeder, W. W., & Wiseman, W. J. (1986). Low-frequency shelf-estuarine exchange processes in Mobile Bay and other estuarine systems on the northern Gulf of Mexico. *Estuarine Variability*, 355–367. https://doi.org/10.1016/b978-0-12-761890-6.50027-7

Seddon, J. (1900). River hydraulics. *Transactions of the American Society of Civil Engineers*, *43*, 217–229.

Sholtes, J. S., & Doyle, M. W. (2011). Effect of channel restoration on flood wave attenuation. *Journal of Hydraulic Engineering*, *137*(2), 196–208. https://doi.org/10.1061/(asce)hy.1943-7900.0000294

Smith, C. G., Osterman, L. E., & Poore, R. Z. (2013). an examination of historical inorganic sedimentation and organic matter accumulation in several marsh types within the Mobile Bay and Mobile—Tensaw River Delta Region. *Journal of Coastal Research*, *63*, 68–83. https://doi.org/10.2112/SI63-007.1

Smith, W. E. (1988). In E. A. Mancini (Ed.), *Geomorphology of the Mobile Delta*. Tuscaloosa, AL: Geological Survey of Alabama.

Sriwongsitanon, N., Ball, J. E., & Cordery, I. (1998). An investigation of the relationship between the flood wave speed and parameters in runoff-routing models. *Hydrological Sciences Journal*, *43*(2), 197–213. https://doi.org/10.1080/02626669809492118

Syvitski, J. P. M., & Saito, Y. (2007). Morphodynamics of deltas under the influence of humans. *Global and Planetary Change*, *57*(3-4), 261–282. https://doi.org/10.1016/j.gloplacha.2006.12.001

Szabo, M. W., Osborne, E. W., Copeland, C. W. Jr., & Neathery, T. L. (1988). Geologic Map of Alabama (Special Map 220). Alabama: Geological Society of Alabama.

Tsai, C. W. (2005). Flood routing in mild-sloped rivers—Wave characteristics and downstream backwater effect. *Journal of Hydrology*, *308*(1-4), 151–167. https://doi.org/10.1016/j.jhydrol.2004.10.027

Turner-Gillespie, D. F., Smith, J. A., & Bates, P. D. (2003). Attenuating reaches and the regional flood response of an urbanizing drainage basin. *Advances in Water Resources*, *26*(6), 673–684. https://doi.org/10.1016/S0309-1708(03)00017-4

United Nations (2017). Factsheet: People and oceans, The Ocean Conference.

U. S. Fish and Wildlife Service (1998). The Mobile River Basin, United States Fish and Wildlife Service.

U. S. Fish and Wildlife Service (2019). National Wetlands Inventory website, United States Department of the Interior, Fish and Wildlife Service, Washington, D.C. http://www.fws.gov/wetlands/

U.S. Geological Survey, U.S. Department of Agriculture - Natural Resource Conservation Service, U.S. Environmental Protection Agency (2019). USGS Watershed Boundary Dataset (WBD) for 2-digit Hydrologic Unit - 03. https://www.sciencebase.gov/catalog/item/5a1632b3e4b09fc93dd171e2

Waldon, M. G., & Bryan, C. F. (1999). In L. P. Rozas, J. A. Nyman, C. E. Proffitt, N. N. Rabalais, D. J. Reed, & R. E. Turner (Eds.), *Annual salinity and nutrient budget of Lake Pontchartrain and impact of the proposed Bonnet Carre diversion*. Baton Rouge: Louisiana Sea Grant College Program.

Waselkov, G. A., Andrus, C. F., & Plumb, G. E. (2016). A state of knowledge of the natural, cultural, and economic resources of the greater Mobile-Tensaw River area, U.S. Department of the Interior.

Webb, B. M., & Marr, C. (2016). Spatial variability of hydrodynamic timescales in a broad and shallow estuary: Mobile Bay, Alabama. *Journal of Coastal Research*, *32*(6), 1374–1388. https://doi.org/10.2112/JCOASTRES-D-15-00181.1

Wolff, C. G., & Burges, S. J. (1994). An analysis of the influence of river channel properties on flood frequency. *Journal of Hydrology*, *153*(1-4), 317–337. https://doi.org/10.1016/0022-1694(94)90197-x

Woltemade, C. J., & Potter, K. W. (1994). A watershed modeling analysis of fluvial geomorphologic influences on flood peak attenuation. *Water Resources Research*, *30*(6), 1933–1942. https://doi.org/10.1029/94WR00323

Yang, K., Cao, S., & Knight, D. W. (2007). Flow patterns in compound channels with vegetated floodplains. *Journal of Hydraulic Engineering*, *133*(2), 148–159. https://doi.org/10.1061/ASCE0733-9429200713:2148

Reference From the Supporting Information

Granato, G. (2012). Estimating basin lagtime and hydrograph-timing indexes used to characterize stormflows for runoff-quality analysis, United States Geological Survey. http://pubs.usgs.gov/sir/2012/5110/